

國立臺灣大學生命科學院動物學研究所

碩士論文

Graduate Institute of Zoology, College of Life Science


National Taiwan University

Master Thesis

研究造成原發性肢端紅痛症

之突變鈉離子通道 $\text{Na}_v1.7$ 其功能性影響

Functional Implications of Mutant $\text{Na}_v1.7$ Channels,
which are Responsible for Primary Erythromelalgia



吳敏慈

Min-Tzu Wu

指導教授：嚴震東、李銘仁、陳志成 博士

Advisors: Chen-Tung Yen, Ph.D.

Ming-Jen Lee, M.D., Ph.D.

Chih-Cheng Chen, Ph.D.

中華民國 101 年 6 月

June, 2012

國立臺灣大學碩士學位論文
口試委員會審定書

研究造成原發性肢端紅痛症之突變鈉離子通道
Na_v1.7 其功能性影響

Functional Implications of Mutant Nav1.7
Channels, which are Responsible for Primary
Erythromelalgia

本論文係吳敏慈君（學號 R99B41003）在國立臺灣大學
動物學研究所完成之碩士學位論文，於民國 101 年 6 月 19 日
承下列考試委員審查通過及口試及格，特此證明

口試委員：嚴震東 陳志斌 李銘仁（簽名）

剛明源（指導教授）

動物學研究所所長 潘建源（簽名）

Acknowledgement

It would not have been possible to write this master thesis without the help and support of the kind people around me. I would like to thank my advisors for their guidance in study design and assistants in thesis writing. Thanks to all the lab members for helping me with experiments. Thanks to my friends who have made my graduate experience joyful and memorable. Lastly and most importantly, I would like to thank my parents for their loving support. I would not have the achievement today without them.



摘要

原發性肢端紅痛症是一種自體顯性遺傳的神經疾病，其病症為肢端的灼燒疼痛感，此症狀會經由外在環境溫熱或運動刺激所引起。目前已發現電壓門控鈉離子通道 $\text{Na}_v1.7$ 上之 α -subunit 的突變(基因為 *SCN9A*)，是導致肢端紅痛症的主要原因，此病症同時也是第一個由基因突變所致的遺傳性神經疼痛症。在台灣我們最近發現三個 *SCN9A* 錯義突變，其中一個為家族遺傳性(I136V)，兩個為偶發性突變(I848T, V1316A)，這當中 V1316A 是尚未被報導過的突變。I136V 突變位置在第一區之第一穿膜區段(DIIS1)，I848T 及 V1316A 分別位在第二及第三區之第四、五穿膜連接區段(DIIS4/S5, DIIS4/S5)。為了瞭解這些突變鈉離子通道的分子病理，我們使用中國倉鼠卵巢細胞進行全細胞電生理記錄。這些突變之鈉離子通道皆在電壓依賴性活化產生過極化偏移，在穩定快速去活化表現出去極化偏移，且比起原生型，突變通道能更快從去活化恢復。由於熱會引發並加劇病症，藉由降低患部溫度病人能得到紓緩，我們於是進而比較溫度(25°C 及 35°C)對原生型與突變鈉離子通道的影響。在 35°C，I136V 及 V1316A 突變通道比起原生型，在電壓依賴性活化仍產生過極化偏移，即使原生型通道本身比起在 25°C 時已有顯著之過極化偏移。升溫則在三個突變通道之穩定去活化皆產生顯著去極化偏移，但原生型通道並不受影響。這些特性改變都可能造成所表達的神經細胞過度興奮，特別是在溫度提昇的狀態下更是如此。由於目前對於肢端紅痛症尚無絕對有效的治療方法，我們試圖利用電生理的方式替帶有這三種突變的病人篩選治療藥物，藉由分析突變型與原生型 $\text{Na}_v1.7$ 通道對 lidocaine 及 mexiletine 抑制效果的 IC_{50} ，我們發現 lidocaine 很可能不適合用來治療這些病人，而如同臨床觀察所示，mexiletine 用於治療帶有 I848T 突變的病人有減緩症狀的功效，如同 I848T 突變型通道展現對 mexiletine 抑制較低的 IC_{50} 。本研究中我們報導一個嶄新的突變，V1316A，同時也提供這些突變鈉離子通道受到升溫影響的分子機制，這些將有助於了解肢端紅痛症的症狀表現，且對於發展有效治療方法也將有所助益。

關鍵字：肢端紅痛症、SCN9A、電壓門控鈉離子通道

Abstract

Primary erythromelalgia (PE) is an autosomal dominant neurological disorder characterized by severe burning pain and erythema in the extremities upon heat stimuli or moderate exercise. Mutations in human *SCN9A* gene, which encodes the α -subunit of the voltage-gated sodium channel, *Nav1.7*, were found to be responsible for PE. Three missense mutations of *SCN9A* gene have recently been identified in Taiwanese patients including a familial (I136V) and two sporadic mutations (I848T, V1316A). V1316A is a novel mutation that has not been characterized. Topologically, I136V is located in DI/S1 segment of the sodium channel, and both I848T and V1316A are located in S4-S5 linker region of DII and DIII domains, respectively. To characterize the electrophysiological properties of these mutant channels, we over-expressed the mutant and wild type channels in Chinese Hamster ovary (CHO-K1) cells and employed the whole-cell patch clamp recordings. The mutant channels showed hyperpolarizing shift in voltage dependent activation, depolarizing shift in steady-state fast inactivation, and faster recovery from inactivation as compared with wild type channel. Since warmth can trigger and exacerbates symptoms and patients can relieve pain by cooling the affected areas, the electrophysiological properties of these mutant and wild type channels at room temperature, 25°C and at a higher one, 35°C were evaluated. At 35°C, I136V and V1316A mutant channels still exhibit a further hyperpolarizing shift in activation as compared with wild type channel, even though wild type channel also produced a significant hyperpolarizing shift compared to that of 25°C. Increased

temperature resulted in significant depolarizing shift in steady-state fast inactivation in all three mutant channels except for the wild type channel. These property changes may contribute to hyperexcitability of sensory neurons that express these mutant channels, especially at high temperature. To search for an effective treatment for these patients, we tested the IC_{50} values of selective sodium channel blockers such as lidocaine and mexiletine. The mutant channels exhibited higher IC_{50} values for lidocaine compared to wild type channel, which suggests that lidocaine would not be a suitable treatment choice. IC_{50} for mexiletine is lower for I848T mutant channel. The result is in part comparable to clinical observations that mexiletine alleviates symptoms in the patients with I136V and I848T mutations but not the patient with V1316A mutation.

Key words: Erythromelalgia; *SCN9A*; $Na_v1.7$

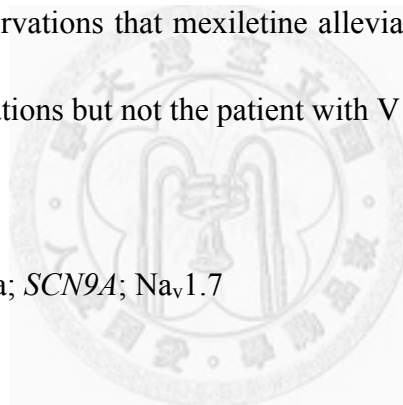


Table of Contents

口試委員會審定書.....	i
Acknowledgement.....	ii
中文摘要.....	iii
Abstract.....	iv
Table of Contents.....	vi
Chapter 1. Introduction.....	1
1.1 Background of erythromelalgia.....	1
1.2 Genetic basis of primary erythromelalgia.....	2
1.3 Molecular biology of voltage-gated sodium channel α -subunits.....	3
1.4 Functional effects of $\text{Na}_v1.7$ mutations.....	5
1.5 Other $\text{Na}_v1.7$ channelopathies.....	8
1.6 Aim of the study.....	11
Chapter 2. Patients, Materials and Methods.....	13
2.1 Study patients.....	13
2.1.1 Patient A.....	13
2.1.2 Patient B.....	14
2.2 Genetic analysis.....	14
2.3 Expression constructs.....	15
2.4 Cell line transfection.....	16
2.5 Whole-cell patch clamp recordings.....	17
2.5.1 Current-voltage relationship.....	17
2.5.2 Steady-state fast inactivation.....	18
2.5.3 Inactivation recovery rate.....	19

2.5.4 Drug antagonism.....	19
2.5.5 Temperature effect.....	20
2.6 Chemicals and solutions.....	20
2.7 Statistics.....	21
Chapter 3. Results.....	22
3.1 Genetic analysis.....	22
3.2 Current-voltage relationship.....	24
3.3 Inactivation curves and inactivation recovery rate.....	25
3.4 Temperature effect.....	26
3.5 Drug antagonism.....	27
Chapter 4. Discussion.....	30
4.1 Genetic analysis.....	30
4.2 Basic electrophysiological properties.....	32
4.3 Temperature effect.....	34
4.4 Drug antagonism.....	36
4.5 Conclusion and future development.....	37
References.....	39
Figures.....	47
Figure 1. Schematic drawing of human Na _v 1.7.....	47
Figure 2. Cloning strategies of hSCN9A full-length cDNA.....	48
Figure 3. Sequence chromatography.....	50
Figure 4. Protein sequence alignments of human Na _v subtypes.....	51
Figure 5. Protein sequence alignments of Na _v 1.7 of various species.....	52
Figure 6. Current-voltage relationships and activation curves.....	53
Figure 7. Steady-state fast inactivation curves.....	55

Figure 8. Inactivation recovery rate.....	56
Figure 9. Activation curves at 25°C and 35°C.....	57
Figure 10. Inactivation curves at 25°C and 35°C.....	59
Figure 11. Lidocaine IC ₅₀ curves.....	60
Figure 12. Mexiletine IC ₅₀ curves.....	61
Figure 13. Use-dependent effect of mexiletine.....	62
Tables.....	63
Table 1. Summary of temperature effect.....	63
Table 2. Summary of mutations located at S4/S5 linker regions.....	64
Table 3. IC ₅₀ values of lidocaine and mexiletine.....	65
Appendix I.....	66



Chapter 1

Introduction

1.1 Background of erythromelalgia

Erythromelalgia (or erythermalgia; OMIM 133020) is a rare neurovascular pain disorder characterized by intermittent severe burning pain, erythema and elevation of temperature in the extremities. It was first named and described in 1878 by Dr. Mitchell (Mitchell 1878). The symptoms are usually bilateral and symmetrical, and they are most often confined in lower extremities but can extend to hands and sometimes earlobes and nose tip (Drenth et al. 2001). There are two forms of erythromelalgia, primary and secondary. Primary erythromelalgia (PE, or inherited erythromelalgia, IEM) can be hereditary or sporadic and it is inherited in an autosomal dominant manner. Secondary erythromelalgia can be associated with a wide variety of conditions including myeloproliferative disorders, peripheral neuropathy, diabetes mellitus, autoimmune and infectious diseases (Drenth et al. 1994). The age of onset for PE is usually before the first decade of life (as early as months after birth) but can also be adult onset (Dib-Hajj et al. 2006). The symptoms appear to persist and progressively worsen through out life for most patients, although some patients reported to show improvement even complete resolution of symptoms (Davis et al. 2000). The painful attacks can be evoked by warm

stimuli and moderate exercises. It was described that the critical temperature lies within the range of 32 - 36°C (Babb et al. 1964). Patients therefore are compelled not to wear socks or closed shoes even in winter. An attack can last from minutes to hours and even days in some cases. Patients can relieve symptoms by elevating affected limbs or submerging affected areas in cold water but by doing so too often, patients might suffer from skin infections. There has not been an effective treatment for PE. In a report of 168 patients with erythromelalgia, 84 medications or treatments (sodium channel blockers, sympathetic blocks, etc.) were used and showed high variability and no treatment is consistently effective (Davis et al. 2000; Hisama et al. 2006).

1.2 Genetic basis of primary erythromelalgia

Genetic linkage locus was first identified at chromosome 2 from a large kindred of five generations with multiple family members affected with PE (Drenth et al. 2001). Analysis of recombination events identified the D2S2370 and D2S1776 as flanking markers in chromosome 2q31-32 and narrowed down to a 7.94 cM interval. (Drenth et al. 2001) Subsequently Yang *et al.* (2004) performed linkage analysis in another affected family of three generations and further refined the linkage to a 5.98 cM region in chromosome 2q24.2-q24.3. By sequencing the selected candidate genes in the linked region, two missense mutations (I848T, L858F) were found in *SCN9A* gene in the

family and a sporadic patient with PE. Family segregation and further screening in normal controls confirmed that mutations in the *SCN9A* are responsible for PE (Yang et al. 2004). Human *SCN9A* gene contains 26 exons and encodes for the α -subunit of voltage-gated sodium channel, $Na_v1.7$. To date 19 mutations in *SCN9A* gene have been reported relating to PE, including 18 missense mutations causing single amino acid substitution and one in-frame deletion. The mutations are shown in Fig. 1. The penetrance is nearly 100% for PE mutations. However, genetic analysis in a family from USA with autosomal dominant primary erythromelalgia did not show a linkage to chromosome 2q (Burns et al. 2005). It is possible that there are other causative genes or there might be mutations in noncoding region of *SCN9A* that result in up-regulation of the channel (Dib-Hajj et al. 2007; Burns et al. 2005).

1.3 Molecular biology of voltage-gated sodium channels

Voltage-gated sodium channel (Na_v) comprises of a family of nine structurally related pore forming α -subunits ($Na_v1.1 - 1.9$) and a family of accessory β -subunits ($\beta1 - \beta4$). These channels are encoded by *SCN1A - SCN5A* and *SCN8A - SCN11A* genes for the α -subunits, and *SCN1B - SCN4B* genes for the β -subunits. Although α -subunits can function alone, they are usually associated with auxiliary β -subunits. The β -subunit is an ~35 kDa transmembrane protein with a single transmembrane domain and an

extracellular immunoglobulin-like domain. It is important in anchoring voltage-gated sodium channels to cell membrane and modulating channel gating and kinetics (Catterall et al. 2005). The α -subunit is an ~260 kDa pore forming protein consist of four homologous domains (DI – DIV) and six transmembrane segments (S1 – S6) in each domain. Positively charged amino acids, lysine or arginine are found at intervals of three amino acids to produce a linear array of positive charges in the S4 segments, which act as voltage sensors (Wood et al. 2004). The membrane re-entrant loops between segments S5 and S6 form the channel pore and selectivity filter. Upon membrane depolarization, the voltage sensors, S4 segments spiral outward causing conformational change and opening of the channel pore (Catterall 2000; Wang et al. 2011). Following activation, sodium channels quickly inactivate to prevent further ion flow through the pore and to allow repetitive action potential firing of cells (Wang et al. 2011). The intracellular loop connects domain III and IV containing the isoleucine-phenylalanine-methionine (IFM) motif, which is responsible for the channel inactivation. The IFM motif acts as a “hinged-lid” that blocks the channel pore upon pore opening (West et al. 1992; Catterall 2005).

The α -subunits can be further subdivided into three groups according to protein sequence, function, and sensitivity to tetrodotoxin (TTX) inhibition. The first group

includes four neuronal sodium channels that are sensitive to nanomolar concentrations of TTX (TTX-S). They are $Na_v1.1$ and $Na_v1.2$ expressed in the central nervous system (CNS), widely distributed $Na_v1.3$ and peripheral $Na_v1.7$. The second group consists of TTX resistant (TTX-R) $Na_v1.5$ in cardiac muscle and $Na_v1.8$, $Na_v1.9$ in nociceptive neurons. The third group includes TTX-S $Na_v1.4$ in skeletal muscle, and $Na_v1.6$ primarily expressed in central and peripheral axons (Rogers et al. 2006).

1.4 Functional effects of $Na_v1.7$ mutations

$Na_v1.7$ is composed of 1977 amino acids (~225 kDa), which is predominantly expressed in dorsal root ganglion (DRG) neurons and sympathetic ganglion neurons (Toledo-Aral et al. 1997). $Na_v1.7$ channel produces rapid activating and inactivating current that is sensitive to TTX blockade. In the DRG, $Na_v1.7$ is concentrated in small C fiber nociceptors and to a lesser extent in medium-sized $A\delta$ and large $A\beta$ cells (Djouhri et al. 2003). Immunohistochemical studies showed that $Na_v1.7$ is present at the distal ends of neurites, close to the impulse trigger zone where neuronal firing is initiated (Drenth & Waxman 2007). $Na_v1.7$ is characterized by slow recovery from inactivation and slow closed-state inactivation, which allows $Na_v1.7$ channels to respond to slow ramp depolarizations and amplify generation potentials at nerve terminals (Cummins et al. 1998; Drenth & Waxman 2007). $Na_v1.7$ therefore is like a “threshold channel” that

amplifies small, subtle depolarizations and brings membrane potential to more depolarized state to activate $\text{Na}_v1.8$, which is responsible for most of the rising phase of action potentials. $\text{Na}_v1.7$ is poised as a molecular gatekeeper of pain detection at peripheral nociceptors (Drenth & Waxman 2007).

Thus far, 17 mutations (as shown in Fig. 1, except for N395K, Q875E, and novel mutation, V1316A) relating to PE have been characterized and all mutant $\text{Na}_v1.7$ channels exhibit significant hyperpolarizing shift in voltage dependent activation compared with wild type channel (Choi et al. 2006; Han et al. 2009; Cheng et al. 2008; Estacion et al. 2010; Ahn et al. 2010; Lampert et al. 2006; Fischer et al. 2009; Choi et al. 2010b; Lampert et al. 2009; Cummins et al. 2004; Han et al. 2007; Harty et al. 2006; Choi et al. 2009; Cheng et al. 2011; Cheng et al. 2010; Waxman & S. Dib-Hajj 2005). The mutant channels also produce depolarizing shift in steady-state fast inactivation (Fischer et al. 2009; Choi et al. 2010b; Lampert et al. 2009; Han et al. 2007; Harty et al. 2006; Waxman & S. Dib-Hajj 2005), slow inactivation (Choi et al. 2006; Han et al. 2009; Cheng et al. 2008; Estacion et al. 2010; Ahn et al. 2010; Lampert et al. 2006; Fischer et al. 2009; Cummins et al. 2004; Cheng et al. 2011; Waxman & Dib-Hajj 2005), slow deactivation (Choi et al. 2006; Cheng et al. 2008; Estacion et al. 2010; Ahn et al. 2010; Lampert et al. 2006; Fischer et al. 2009; Lampert et al. 2009; Cummins et al.

2004; Han et al. 2007; Harty et al. 2006; Choi et al. 2009; Cheng et al. 2011), and increased ramp current (Cheng et al. 2008; Estacion et al. 2010; Choi et al. 2006; Ahn et al. 2010; Lampert et al. 2006; Fischer et al. 2009; Lampert et al. 2009; Cummins et al. 2004; Han et al. 2007; Harty et al. 2006; J. Choi et al. 2009; Cheng et al. 2011; Cheng et al. 2010). These channel property changes may render DRG neurons hyperexcitability. Studies in DRG neurons in deed showed that mutant $Na_v1.7$ channels depolarized resting membrane potential (Choi et al. 2010b; Harty et al. 2006), lowered the threshold for action potential firing, and enhanced repetitive firing (Han et al. 2009; Choi et al. 2010b; Han et al. 2007; Harty et al. 2006; Cheng et al. 2011; Cheng et al. 2010; Waxman & S. Dib-Hajj 2005).

While these mutant $Na_v1.7$ channels render the DRG neuron hyperexcitability, it was demonstrated by Rush *et al.* (2006) that in sympathetic neurons they may have the opposite effect. L858H mutant channel was transfected into rat DRG neurons and superior cervical ganglion (SCG) neurons to characterize the electrophysiological properties. As seen in other mutant channels, L858H mutant channels produce depolarization of resting membrane potential, decrease action potential threshold, and enhance repetitive firing in DRG neurons. On the other hand, L858H mutant channels in SCG neurons also produce depolarization of resting membrane potential, but increase

action potential threshold, and attenuate repetitive firing. The opposing effects might be due to the selective presence of $\text{Na}_v1.8$ in sensory but not sympathetic neurons. The voltage dependent activation and steady-state fast inactivation are more depolarized for $\text{Na}_v1.8$, which allow it to remain available even at depolarized membrane potential induced by L858H in DRG neurons. In SCG neurons only $\text{Na}_v1.3$, $\text{Na}_v1.6$, and $\text{Na}_v1.7$ are present and they would be inactivated by the depolarizing shift in resting membrane potential. It was evidenced that when co-expressed $\text{Na}_v1.8$ and L858H mutant channels in SCG neurons, increased excitability was observed. This study provided a molecular basis for the sympathetic dysfunction that has been observed in PE (Rush et al. 2006).

Temperature is a critical factor for triggering the clinical features of PE. Han *et al.* (2007) investigated the effect of temperature on the gating properties of L858F mutant $\text{Na}_v1.7$ channel. They found that cooling differentially shifts the midpoint of steady-state activation in depolarizing direction for L858F but not for wild type channels, which is likely to contribute to the alleviation of painful symptoms upon cooling in affected limbs in PE patients (Han et al. 2007).

1.5 Other $\text{Na}_v1.7$ channelopathies

Paroxysmal extreme pain disorder (PEPD; OMIM 167400), previously known as familial rectal pain syndrome (Fertleman & Ferrie 2006), is also an autosomal dominant pain disorder caused by gain-of-function mutations in *SCN9A* gene. It is characterized by episodic burning pain in rectal, ocular, and mandibular areas with skin flushing of the lower limbs, in a uni- or bi-lateral fashion (Fertleman et al. 2006; Fertleman et al. 2007). Rectal pain can be triggered by defecation or probing of the anal or genital areas; while eating, irritations or cold can trigger symptoms in ocular and mandibular areas (Dib-Hajj et al. 2007). Most mutations related to PEPD reside in the fast-inactivation peptide (IFM, in intracellular loop between domain III and IV) and the intracellular linker regions between S4-S5 of domain III and IV, which act as receptor for inactivation gate (Drenth & Waxman 2007). Three mutations (I1461T, T1461I, and M1627K), which characterized in whole-cell patch clamp studies and showed impaired fast inactivation and persistent current (I1461T and T1461I), as well as depolarizing shift in voltage dependency of steady-state inactivation (M1627K) (Fertleman et al. 2006). These PEPD related mutations have no (or in relatively small degree) effects on channel activation as oppose to mutations relating to PE. Most PEPD patients therefore respond well to carbamazepine treatment, which selectively targets and stabilizes the inactivated state of sodium channels, whereas carbamazepine is less effective in PE patients. However, not all PEPD patients show favorable response to carbamazepine. A

recently reported mutation (G1607R) located at voltage sensor S4 of domain IV, causes a depolarizing shift in steady-state inactivation with persistent sodium current which cannot be alleviated by carbamazepine (Choi et al. 2010a).

Another pain disorder linked to *SCN9A* gene is channelopathy-associated congenital insensitivity (or indifference) to pain (CIP; OMIM 243000). It is caused by loss-of-function mutations (homozygous or compound heterozygous of nonsense and/or deletion mutations that result in non-functional truncated protein) and is an autosomal recessive transmission in families. These patients typically do not experience any form of pain all over their bodies including visceral pain since birth. They experience painless burns, bone fractures, and mostly have severe injuries to their lips and/or tongues due to biting during infancy. Despite the expression of Na_v1.7 in sympathetic ganglion neurons is absent in CIP patients, they have normal axon-reflex response and no apparent deficit in autonomic function (Dib-Hajj et al. 2007; Cox et al. 2006). It has recently been reported that patients with CIP lack the sense of smell, which indicates a functional role of Na_v1.7 in olfaction (Weiss et al. 2011).

Last year there was a study reported for the first time that gain-of-function mutations in *SCN9A* gene are associated with idiopathic small fiber neuropathy (I-SFN) (Faber et al.

2011). Eight out of 28 patients (28.6%) with I-SFN were screened positive for novel mutations in *SCN9A* and subsequent electrophysiological analyses revealed multiple gain-of-function changes in the mutant channels. Each of the mutations confers to the hyperexcitable DRG neurons. The results suggest an etiological basis for I-SFN, whereby expression of gain-of-function mutant $\text{Na}_v1.7$ channels in small diameter peripheral axons, may cause these fibers to degenerate (Faber et al. 2011).

1.6 Aim of the study

Three missense mutations in *SCN9A* gene were identified in Taiwanese patients including one familial (I136V) and two sporadic mutations (I848T, V1316A). The familial mutation, isoleucine 136 changed to valine (I136V), was reported by Lee *et al.* (2007), and subsequently characterized with whole-cell patch clamp by Waxman *et al.* (2008) The proband was a 21-year-old male at the time of report. He first observed symptoms affecting bilateral feet at age of 11 years, and subsequently his hands began showing milder symptoms around age of 19 years. Elevation of environmental or body temperature, exercising, or wearing shoes would trigger attacks and worsen the symptoms. Cooling the affected areas by immersion in cold water tended to relieve the pain (Lee et al. 2007). Isoleucine 136 is located at the first transmembrane segment of domain I (DI/S1) of $\text{Na}_v1.7$. The mutation is due to a transversion from “A” to “G” at

nucleotide 406 in exon 3 (reference sequence GeneBank NM_002977), which resulted in a substitution of valine136 for isoleucine. I136V mutant $Na_v1.7$ channel was characterized in HEK293 cells and it appears to shift the voltage dependent activation in hyperpolarizing direction, decrease the deactivation rate, and generate larger ramp currents.

In this study we also report a sporadic mutation, I848T as well as a novel mutation, V1316A in *SCN9A* gene from Taiwanese patients. Together with I136V mutant channel, we characterized the basic electrophysiological properties and evaluated how increased temperature can modulate the gating properties of these mutant channels in CHO-K1 cells. In addition, since treatments for PE have only been partially successful and seem to be mutation specific, we assessed the differential inhibition of sodium channel blockers on these mutant channels and using the electrophysiological parameters as a tool to screen for the potential treatments in these patients.

Chapter 2

Patients, Materials and Methods

2.1 Study patients

Three mutations have recently been identified in Taiwanese patients who were diagnosed with primary erythromelalgia. The diagnostic criteria for erythromelalgia include: 1) burning extremity pain, 2) pain aggravated by warming, 3) pain relieved by cooling, 4) erythema of the affected skin, and 5) increased temperature of the affected skin (Thompson et al. 1979; Drenth et al. 1994). Differential diagnosis including reflex sympathetic dystrophy, Fabry's disease, and other painful neuropathies associated with diabetes mellitus, alcoholism, HIV infection and Lyme disease were excluded.

2.1.1 Patient A

Patient A is a 33-year-old female who came to Dr. Ming-Jen Lee's clinic at National Taiwan University Hospital about three years ago. She suffered from burning pain and erythema in her feet since she was eight years old. At hot weather, the feet developed severe burning pain with reddish skin discoloration. Her palms were affected as well in recent decade. Walking and warmth trigger the symptoms, which made difficulties for her to wear shoes and socks. To relieve foot pain, she preferred to have her feet immersed in water and even on ice to gain pain relief. Mexiletine and acetaminophen

have been prescribed with mild improvement in pain scale. There is no family history and her parents are unremarkable.

2.1.2 Patient B

Patient B was a 16-year-old girl when she first visit Dr. Lee's clinic. The chief complaint was the recurrent severe burning pain of both feet since age seven. The symptoms affecting both feet symmetrically, and gradually extended to bilateral knees and hands in recent months. Many various medications such as aspirin, mexiletine, carbamazepine, propranolol, gabapentin, and imipramine have been prescribed but only little effect was observed. To relieve pain, she had to immerse her hands and feet in ice water at night. Nevertheless, prolonged immersion in ice-cold water with small wound resulted in infection associated with blisters and cellulitis. Local heating due to inflammation aggravated the causalgia and burning pain of both feet. Unfortunately, neurogenic shock with collapse took place due to severe pain after debridement.

2.2 Genetic analysis

DNA was extracted from patients' blood using Genomic DNA Extraction Kit (Geneaid, Taipei, Taiwan). Informed consent was signed before blood samples were collected.

Polymerase chain reaction (PCR) was performed in thermal cycler (GeneAmp® PCR

System 2700, Applied Biosystems, CA, USA) for each of the 26 coding exons. Exon primers were designed according to the published sequences (GeneBank NM_002977) as described by Yang *et al.* (2004) The PCR reaction mixture (50 μ l) contains 2 mM dNTP (5 μ l), 10X PCR Buffer (5 μ l), forward primer 10 μ M (3 μ l), reverse primer 10 μ M (3 μ l), 1.25U Taq DNA polymerase (Thermo, MA, USA), dH₂O 27 μ l, and DNA template 100ng. The PCR protocol included an initial cycle of denaturation at 95°C for 15 minutes, followed by 25 cycles of (94°C for 30 seconds, 60°C for 30 seconds decreased by 0.4°C /cycle and 72°C for 45 seconds), 12 cycles of (94°C for 30 seconds, 50°C for 30 seconds and 72°C for 45 seconds) and an extension step at 72°C for 7 minutes. The PCR products were purified with PCR DNA Fragments Extraction Kit (Geneaid, Taipei, Taiwan), and sequenced using BigDye® sequencing chemistry (version III, Applied Biosystems, CA, USA) and analyzed on an automated ABI3100™ DNA sequencer (Applied Biosystems, CA, USA).

2.3 Expression constructs

The full-length cDNA of human *SCN9A* gene was purchased from OriGene company (OriGene Technologies, Rockville, MD, USA). It was first cloned into pTracer-EF/V5-His A vector (Invitrogen, Life Technologies, NY, USA) using NotI cloning site (Fig. 2A). The GFP sequence that is driven by a separate promoter in

pTracer vector allows visual identification of transfected cells when performing electrophysiological recordings. Because of the large size of SCN9A cDNA (~6.4 kb), short segments containing regions of point mutations were subcloned into pBluescript vector for mutagenesis (Fig. 2B), which was done using Site-Directed Mutagenesis Kit (Stratagene, Agilent Technologies, CA, USA). After successful mutagenesis, each mutation-containing segment was cloned back to full-length SCN9A cDNA. To amplify, pTracer-SCN9A (both wild type and mutant) plasmids have to be transformed into JM109 competent cells and must be cultured at 30°C in standard ampicillin (100 µg/ml) containing LB media. Sodium channel β-subunit construct, pIRES-hSCN1B/2B, was provided by Dr. Chih-Cheng Chen's laboratory (IBMS, Academia Sinica, Taipei, Taiwan). The map is as shown in Appendix I.

2.4 Cell line transfection

CHO-K1 (Chinese Hamster Ovary) cells (Food Industry Research and Development Institute, Hsinchu, Taiwan) were cultured under the standard condition (5% CO₂; 37°C) in F12 medium (Gibco®, Life Technologies, NY, USA) supplemented with 10% fetal bovine serum (Gibco®, Life Technologies, NY, USA). The wild type and mutant SCN9A constructs (wild type or mutant) were co-transfected with the pIRES-SCN1B/2B β-subunit construct, in 1:3 ratio using Lipofectamine™ 2000

(Invitrogen, Life Technologies, NY, USA). Electrophysiology recordings were done within 24 - 48 hours post-transfection.

2.5 Whole-cell patch-clamp recordings

Whole-cell patch-clamp recordings were conducted at room temperature (23-25°C) except for the temperature effect experiment, which is described in later section. Glass pipettes (Warner Products 64-0792, CT, USA) were prepared (7–9 M Ω) with use of a vertical puller (NARISHIGE PP-830, Tritech Research, Inc., CA, USA). The Axopatch MultiClamp 700B (Axon Instruments, Molecular Devices, CA, USA) was employed for whole-cell recording experiments. The stimuli and the digital records captured would be performed with use of the Signal 3.0 software and a CED1401 converter (Cambridge Electronic Design, Cambridge, England). Currents were sampled at a rate of 10 kHz and filtered at 3 kHz. The pipette solution contained (in mM): 10 NaCl, 110 CsCl, 20 TEA, 2.5 MgCl₂, 5 EGTA, 3 ATP, 5 HEPES, pH 7.0 (adjusted with CsOH), and the osmolarity was adjusted to 300 (\pm 10) mOs-mol/L with glucose. The extracellular bath solution contained (in mM): 100 NaCl, 5 CsCl, 30 TEA, 1.8 CaCl₂, 1 MgCl₂, 0.1 CdCl₂, 5 HEPES, 25 Glucose, 5 4-aminopyridine, pH 7.4 (adjusted with CsOH or MES), and the osmolarity was adjusted to 300 (\pm 10) mOs-mol/L with glucose.

2.5.1 Current-voltage relationship

To record current-voltage relationship, after establishing whole-cell condition (with leak current < 300 pA), cells were held at -100 mV and stepped to a range of potentials (-80 to +30 mV in 5 mV increments) for 50 ms. I-V curves were generated by plotting normalized peak currents (I/I_{\max}) as a function of depolarization potential. To obtain activation curves, peak currents (I) were first converted to conductance (G) at each voltage potential (V) by using the following equation: $G = I/(V - V_{\text{rev}})$. V_{rev} is the reversal potential, which was determined for each cell individually. It is estimated by linear extrapolation of peak current amplitudes with depolarization potentials from 5 to 30 mV. Normalized conductance (G/G_{\max}) was plotted and fitted with Boltzmann's equation: $G/G_{\max} = 1/\{1 + \exp[(V_{1/2, \text{act}} - V)/k]\}$, where $V_{1/2, \text{act}}$ is the voltage potential of half-maximal activation, and k is the slope factor.

2.5.2 Steady-state fast inactivation

For steady-state fast inactivation study, cells were held at -100 mV and presented a 500 ms pre-pulse (ranging from -140 to +10 mV in 10 mV increment) followed by a 20 ms test pulse of -20 mV. The current measured from the test pulse was normalized with maximal current amplitude (I/I_{\max}) and plotted as a function of depolarizing potential. Plot was then fitted with Boltzmann's equation: $I/I_{\max} = 1/\{1 + \exp[(V_{1/2, \text{inact}} - V)/k]\}$ to

obtain the inactivation curve, where $V_{1/2, \text{inact}}$ is the voltage potential of half-maximal inactivation, and k is the slope factor.

2.5.3 Inactivation recovery rate

To analyze the rate of inactivation recovery, cells were held at -100 mV and a pair-pulse of -20 mV was applied. The time interval between the two pulses (interstimulus interval) was adjusted from 2 to 20 ms in 2 ms increment. The current recorded from the second pulse was normalized to the current recorded from the first pulse. Normalized current was plotted as a function of interstimulus interval and fitted with first-order exponential equation to obtain the recovery time constant, τ (tau).

2.5.4 Drug antagonism

For drug antagonism study, extracellular solutions with various concentrations of drug were perfused through the recording chamber. Cells were held at -100 mV and stimulated with a 50 ms depolarizing pulse of -20 mV under treatment of drug and repeating the recording until the drug had been washed out. Percent of remaining current was then calculated as current recorded when treated with drug (I_{drug}) divided by that after wash (I_{wash}). The dose-response curve was fitted with the following logistic equation: $I_{\text{drug}}/I_{\text{wash}} = 1 / [1 + IC_{50}/M]^n$, where IC_{50} is the concentration that results in 50%

inhibition, M is the concentration of drug, n is the Hill coefficient. To assess use-dependent inhibition of mexiletine, cells were given repeated 50 ms depolarizing pulses of -20 mV from -100 mV holding potential at a frequency of 5 Hz in 6 seconds duration (total 30 pulses) with absence or presence of mexiletine. Current amplitude from each pulse was normalized to the maximal current (first pulse) measured with absence of mexiletine.

2.5.5 Temperature effect

The temperature of recording chamber was controlled at 25°C and 35°C with Badcontroller V (Luigs & Neumann, Ratingen, Germany). The accuracy of controller is $\pm 0.1^\circ\text{C}$ at 37°C, and $\pm 0.2^\circ\text{C}$ between 0°C to 60°C. The flow rate of external solution was 0.3 ml/min and the volume of recording chamber was approximately 3 ml. With such slow flow rate, the temperature fluctuation was minimal.

2.6 Chemicals and solutions

Lidocaine hydrochloride (L5647, Sigma-Aldrich Corp., MO, USA) and mexiletine hydrochloride (M2727, Sigma-Aldrich Corp., MO, USA) were dissolved in extracellular bath solution to give stock solutions of 100 mM. Subsequent dilutions were performed in extracellular bath solution to give concentrations of (mM): 0.1, 0.3, 1,

3, 10 and 30. Stock solutions were stored at 4°C for no more than three weeks. Working solutions were made fresh before patch-clamp recordings.

2.7 Statistics

Statistics and curve fitting were done using Prism 5 (GraphPad Software, Inc., CA, USA), except for the IC₅₀ curves, which were fitted using Origin 6.0 (OriginLab, MA, USA). The unpaired t-test was used to compare data between groups and $P < 0.05$ was considered statistically significant. Data are shown as means \pm SEM.



Chapter 3

Results

3.1 Genetic analysis

Three missense mutations of human *SCN9A* gene, one familial (I136V) and two sporadic mutations (I848T, V1316A) have recently been identified in Taiwanese patients with primary erythromelalgia. Among which, V1316A is a novel mutation that has not been reported before. Human *SCN9A* gene encodes the α -subunit of the voltage-gated sodium channel, $\text{Na}_v1.7$. The sodium channel is composed of four repeated domains (DI~DIV) and in each domain there are six transmembrane segments (S1~S6) (Catterall 2000). Isoleucine136 is located at the first transmembrane segment of domain I (DI/S1) of $\text{Na}_v1.7$ and was identified and described in 2007 by Lee *et al.* (Lee et al. 2007).

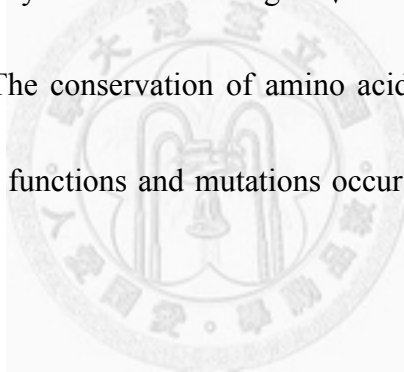
Patient A was a 33 year old female who developed excruciating burning pain at hot weather or in feverish at her young age. There were no symptoms of motor dysfunction. Although severe pain occurred, no hypo-, hyperesthesia or allodynia were found on her feet. She also denied any history of diabetes, autoimmune disease or Raynaud's phenomenon. On examination, the feet were reddish and warm. There were no motor weakness, no muscle atrophy and no sensory loss on all sensory modality. The clinical

electrophysiological data, including nerve conduction, variance of R-R interval and sympathetic skin response tests, were all unremarkable. The blood biochemistry and autoimmune profiles were normal. Given the typical phenotype of primary erythromelalgia, *SCN9A* gene sequencing of patient A showed a “T” to “C” substitution at nucleotide 2543 in exon 15 (reference sequence GeneBank NM_002977), which resulted in a missense mutation of isoleucine848 changing to threonine (Fig. 3A). Isoleucine848 is located in the intracellular linker region between the fourth and fifth transmembrane segments of domain II (DII/S4-S5) as shown in the upper panel of Fig. 4. The same mutation was previously reported in three sporadic cases of Chinese patients and two familial cases (English and French) (Yang et al. 2004; Drenth et al. 2005; Natkunarajah et al. 2009).

Patient B is also a sporadic case, who suffered from the typical phenotype of primary erythromelalgia. The age of onset is at year 7 with progressive course implying a genetic disorder. She could not tolerate the severe feet burning pain but to immerse them with water or ice water. Inflammation with blisters and wounds on skin of both pedal regions ascending to mid-calf level further aggravated the erythromelalgia. Unfortunately, pain with autonomic instability resulted in neurogenic shock and she passed away after debridement. Sequencing of *SCN9A* gene identified a transversion of

nucleotide “T” to “C” change at position 3947 (exon 22) of coding sequence (reference sequence GeneBank NM_002977) (Fig. 3B). The novel mutation, Val1316Ala, is located in the intracellular linker region between fourth and fifth transmembrane segments of domain III (DIII/S4-S5) (Fig. 4).

Sequence alignments show that the amino acids (I136, I848 and V1316), which mutated are highly conserved among human voltage-gated sodium channel α -subunit subtypes (Fig. 4). They are also highly conserved among $\text{Na}_v1.7$ homologs of various species during evolution (Fig. 5). The conservation of amino acids at these positions suggest their importance in channel functions and mutations occur at these positions are likely to alter channel properties.



3.2 Current-voltage relationship

To characterize the electrophysiological properties of these PE related mutant $\text{Na}_v1.7$ channels, both wild type and mutant channels were over-expressed in CHO-K1 cells together with human SCN1B/2B β -subunits. Using whole-cell patch clamp recording, the current-voltage relationships of wild type and mutant channels were recorded (Fig. 6). Cells were held at -100 mV and stepped to a range of potentials (-80 - +30 mV with 5 mV increment) for 50 ms to record the current amplitude that was induced at each

voltage step. The current-voltage (I-V) curves showed that there is a hyperpolarizing shift in voltage dependent activation for mutant channels with no apparent shift in reversal potential (Fig. 6B, C, D). Mutant channels were activated and reached maximal current amplitude at more hyperpolarized potential as compared with wild type channel. To obtain activation curves, normalized conductance was fitted with Boltzmann equation, and the half maximal activation potential (activation $V_{1/2}$) of each channel was calculated (Fig. 6E, F, G). All mutant channels produce a significant ($P < 0.001$) hyperpolarizing shift in activation $V_{1/2}$ compared with wild type channel (-25.88 ± 0.35 mV, $n = 30$) (Fig. 6H). I136V mutant channel has the largest shift (-35.32 ± 0.33 mV, $n = 26$) among all mutant channels (I848T: -30.84 ± 0.39 mV, $n = 25$; V1316A: -32.68 ± 0.44 mV, $n = 31$). The slope factors of activation curves are similar except for V1316A mutant channel (6.01 ± 0.39 , $n = 31$), which has a significant ($P < 0.05$) increase as compared with wild type (Fig. 6I). The result of hyperpolarizing shift of voltage dependent activation in mutant channels would increase the channel sensitivity.

3.3 Steady-state fast inactivation curves and inactivation recovery

Steady-state fast inactivation was tested by subjecting transfected cells to a series of 500 ms pre-pulses (-140 mV to -10 mV with 10 mV increment) and followed by a 20 ms test pulse of -20 mV. Boltzmann fits of normalized current amplitude from test pulses reveal

significant ($P < 0.001$) depolarizing shift in steady-state fast inactivation for all mutant channels compared with wild type (Fig. 7A-D). The half maximal inactivation potential (inactivation $V_{1/2}$) of wild type channel is -75.89 ± 0.41 mV ($n = 14$) (Fig. 7E). There is no apparent difference in slopes for all channels (Fig. 7F).

To assess the channel recovery rate from inactivation back to available state, a pair-pulse of depolarization from -100 to -20 mV was applied. The time interval between two pulses is the interstimulus interval and was adjusted from 2 to 20 ms with 2 ms increment. The percentage of current recovered from inactivation by the first pulse was measured and plotted as a function of time of interstimulus interval. The recovery time constant, τ (tau) was obtained by fitting the plot with first order exponential equation. The recovery τ is 10.7 ms ($n = 6$) for wild type channel (Fig. 8A). All mutant channels recover significantly faster compared with wild type channel with recovery τ of 4.25 ($n = 6$), 5.58 ($n = 7$), 5.29 ms ($n = 5$) for I136V, I848T, and V1316A respectively (Fig. 8B-D). The depolarizing shift of inactivation $V_{1/2}$ and faster recovery would increase the channel activity by allowing channel to remain open at more depolarized potential and being reactivated more rapidly.

3.4 Temperature effect

Since warmth evokes and worsens symptoms in PE patients, and cooling the affected areas patients can feel relieved, we therefore assessed the effect of temperature on wild type and mutant $\text{Na}_v1.7$ channels. Both voltage dependent activation and steady-state fast inactivation were analyzed at 25°C and 35°C (Fig. 9). At 25°C, all the mutant channels have significant ($P < 0.001$) hyperpolarizing shift (I136V: -34.24 ± 0.72 mV, $n = 13$; I848T: -29.6 ± 0.5 mV, $n = 20$; V1316A: -29.78 ± 0.59 mV, $n = 19$) in activation $V_{1/2}$ compared with wild type channel (-22.07 ± 0.31 mV, $n = 29$) (Table 1). Increased temperature significantly ($P < 0.001$) hyperpolarizes the activation $V_{1/2}$ of wild type (-26.22 ± 0.55 mV, $n = 15$), and V1316A (-33.45 ± 0.53 mV, $n = 14$) mutant channel. But, there was no effect on I136V mutant channel (Fig. 9A, B, D). However, both mutant channels still have more hyperpolarized activation $V_{1/2}$ compared with wild type channel (Fig. 9E, Table 1). On the contrary, I848T mutant channel produced a depolarizing shift of ~ 4 mV ($P < 0.001$, $n = 19$) and therefore resulted in no difference from wild type channel (Fig. 9C, E). The activation curves of I848T and V1316A at 25°C were less steep as compared with the wild type channel, whereas at 35°C there is no significant difference between mutant and wild type channels. V1316A mutant channel at 35°C had steeper slope as compared to that at 25°C (Fig. 9F).

Increased temperature does not affect the steady-state inactivation in wild type channel (Fig. 10A). However, the inactivation $V_{1/2}$ of all the mutant channels are further depolarized upon temperature increase (I136V: ~ 3.44 mV, $n = 18$; I848T: ~ 3.3 mV, $n = 21$; V1316A: ~ 1.9 mV, $n = 14$) and therefore result in greater degree of shift compared with wild type channel (Fig. 10E). There is no significant difference in curve slopes. Increased temperature would enhance channel activity especially in mutant $Na_v1.7$ channels.

3.5 Drug antagonism

Currently treatments for PE using sodium channel blockers such as local anesthetics (*e.g.* lidocaine), anti-convulsants (*e.g.* carbamazepine, phenytoin), or tricyclic antidepressants (*e.g.* imipramine) have only been partially successful. We sought to use electrophysiology to screen for drugs that are potentially effective for patients with these three mutations. Normalized peak currents induced by depolarizing from -100 to -20 mV with various concentrations of drugs were measured. By fitting with logistic equation as described previously, the concentration of 50% inhibition (IC_{50}) can be calculated. We first tested the IC_{50} values of a local anesthetic, lidocaine, for wild type and mutant $Na_v1.7$ channels. All three mutant channels seem to be more resistant to lidocaine blockade with significant higher IC_{50} values (I136V: 3.95 ± 1.58 mM, $n = 5$;

I848T: 3.11 ± 0.48 mM, $n = 7$; V1316A: 7.92 ± 2.50 mM, $n = 4$) compared with wild type channel (1.31 ± 0.87 mM, $n = 5$) (Fig. 11). We further tested mexiletine, a sodium channel blocker. As shown in Fig. 12A, wild type channel has an IC_{50} value of 1.77 ± 0.78 mM ($n = 6$). I136V (2.03 ± 0.38 mM, $n = 7$) and V1316A (1.73 ± 0.20 mM, $n = 8$) mutant channels reveal similar IC_{50} values as wild type channel (Fig. 12B, D), while I848T mutant channel results in significant lower (1.08 ± 0.11 mM, $P < 0.05$, $n = 7$) IC_{50} for mexiletine (Fig. 12C, Table 2). Our results indicate that lidocaine is not a suitable treatment choice for these patients.

Since it was reported that these drugs may exert the inhibition effect in a use-dependent manner (Choi et al. 2009), we then examined the use-dependent effect of mexiletine on wild type and mutant channels by stimulating transfected cells with depolarizing pulses from -100 mV holding potential to -20 mV at a frequency of 5 Hz with presence and absence of 1 mM of mexiletine. However, no significant difference was observed between wild type and mutant channels (Fig. 13).

Chapter 4

Discussion

In this study we report a previously identified mutation, I848T that is first found in a Taiwanese PE patient, as well as a novel mutation, V1316A in *SCN9A* gene, which encodes for an α -subunit of voltage-gated sodium channel, $Na_v1.7$. The electrophysiological study shows that these mutations increase the sodium channel activity, which may result in hyperexcitability of sensory neurons. The hyper-activity of mutant $Na_v1.7$ channels can be further enhanced at higher temperature. In search of effective treatment for PE, we found the differential inhibition of sodium channel blockers on these mutant $Na_v1.7$ channels.

4.1 Genetic analysis

The missense mutation, V1316A is a novel mutation. There has not been any mutation or single nucleotide polymorphism (SNP) reported at the same position in other Na_v subtypes and cause diseases, either. The I848T mutation has previously been identified in three sporadic case from China and two familial cases from England and France (Yang et al. 2004; Drenth et al. 2005)³. This is the first report from Taiwanese patient and it occurs most frequent as compared to all the other mutations in *SCN9A* gene

resulting in PE (Fig. 1). It occurs among variable ethnic groups of patients and could probably be a mutation hotspot.

For electrophysiological study, we included all three mutations that were found in Taiwanese patients, which are I848T, V1316A and previously identified familial mutation, I136V. Protein sequence alignments show that these amino acids (I136, I848, and V1316) are highly conserved during evolution and also among other voltage-gated sodium channel α -subunit subtypes, with an exception in I136 (Fig. 4, 5). The corresponding residue of I136 in $\text{Na}_v1.9$ is actually valine, just as our I136V mutant $\text{Na}_v1.7$. $\text{Na}_v1.9$ activates at more hyperpolarized potentials compared to the other sodium channels (reviewed in Cheng et al. 2008), so does I136V mutant $\text{Na}_v1.7$ channel as compared with the wild type channel. It is possible that the corresponding residue of valine shared by I136V mutant $\text{Na}_v1.7$ and $\text{Na}_v1.9$ contributes to the hyperpolarized activation. I136V is located in D1S1 transmembrane segment (Fig. 4, upper panel), which has not been implicated in channel gating. However, it was shown that the S1 – S3 segments form a narrow groove, which voltage sensor S4 slides along in an electric field by interacting with the negatively charged residues in neighboring transmembrane segments (Yarov-Yarovoy et al. 2012)³. The substitution of isoleucine with valine

might alter the conformation of the “groove” and as a result affect the voltage sensing and channel gating.

I848T and V1316A are both located on the intracellular loop linking transmembrane segment S4 and S5 of domain II and III respectively (Fig. 4, upper panel). Upon membrane depolarization, the voltage sensor S4 segment spirals outward and pulls on the S4/S5 linker, which induces movement of S5 and S6 segment and opens the channel pore (Yarov-Yarovoy et al. 2012). Isoleucine is a nonpolar, neutral amino acid. Since threonine harbors a polar side chain, the replacing isoleucine by threonine might cause conformation change. Valine is a nonpolar, neutral, and branched amino acid, while alanine is also nonpolar and neutral but structurally much smaller amino acid. Both mutations, I848T and V1316A located on the S4/S5 linker might change the conformation of the linkers with S5 and S6 segments that is critical for channel gating.

4.2 Basic electrophysiological properties

The mutant Na_v1.7 channels harboring the I136V, I848T, and V1316A mutations resulted in hyperpolarizing shift in voltage dependent activation and depolarizing shift of the inactivation V_{1/2} of steady-state fast inactivation (Fig. 6, 7). Moreover, all three mutant channels recovered significantly faster from inactivation as compared with wild

type channel (Fig. 8). Hyperpolarizing shift of activation threshold and the activation $V_{1/2}$ would increase the channel sensitivity. Only V1316A mutant channel showed change in slope of the activation curve, which was less steep than wild type channel. This is due to the greater hyperpolarizing shift of activation threshold without much shift in the maximum current. Hyperpolarizing shift in activation together with the depolarizing shift in inactivation $V_{1/2}$ might increase the window current which may result in depolarizing resting membrane potential of sensory neurons as previously demonstrated (Choi et al. 2010b; Harty et al. 2006). The faster recovery from inactivation back to available state allows the mutant channels to be reactivated more rapidly than wild type channel, which contributes to hyper-activity of these mutant channels. Since no apparent difference was observed in reversal potential (Fig. 6A, C, E), we reason that the changes in gating property is not due to permeation of other ions. Several mutations related to PE are located at the S4/S5 linker regions (Table 2), but there is no distinct property change in these regions compared with other mutations. It is still unclear why mutations located at different positions result in similar functional changes.

The electrophysiological data such as hyperpolarizing shift in voltage dependent activation for I136V and I848T mutant channels are comparable with previous studies,

but not the steady-state fast inactivation (Cheng et al. 2008; Cummins et al. 2004). It has been reported that no significant shift in inactivation $V_{1/2}$ in both I136V and I848T mutant channels except the steeper slope for I136V inactivation as compared with wild type channel. The discrepancy might be due to different expression systems. The previous studies were performed in HEK293 cells as oppose to CHO-K1 cells in our study. Additionally, the expression construct of $Na_v1.7$ channel used by Cheng *et al.* (2008) and Cummins *et al.* (2004) was converted to TTX-R form, and electrophysiological recordings were conducted with TTX blockade of endogenous sodium current in HEK293 cells. The amino acid change for TTX sensitivity and different cell background might be the reason for different results. Therefore we should only compare our findings to the wild type control in our system.

4.3 Temperature effect

It was reported by Babb et al. (1964) that the critical range of temperature, which triggers the painful attacks in erythromelalgia is 32 - 36°C. Therefore we assessed the gating property change in wild type and I136V, I848T, and V1316A mutant channels at 35°C compared to control of 25°C. In voltage dependent activation, our results showed that increasing temperature would significantly hyperpolarize the activation $V_{1/2}$ of wild type and V1316A mutant $Na_v1.7$ channels. There is no change in I136V mutant channel

with increasing temperature. The activation $V_{1/2}$ of both I136V and V1316A mutant channels were still significantly more hyperpolarized as compared with wild type channel at 35°C. Surprisingly, I848T mutant channel shifted the activation $V_{1/2}$ in depolarizing direction, which results in no significant difference from wild type channel at 35°C. The inactivation $V_{1/2}$ of steady-state fast inactivation was not altered for wild type channel at 35°C. However, increasing temperature further depolarize the inactivation $V_{1/2}$ of all three mutant channels.

Since wild type channel also exhibited hyperpolarizing shift in activation at 35°C, increasing temperature triggers the painful attacks in PE is probably due to the depolarizing of steady-state fast inactivation, which enhances the hyper-activity of mutant channels. In addition, I136V has more hyperpolarized activation $V_{1/2}$ compared with wild type. Among three mutations, only V1316A mutant channel produced both hyperpolarizing shift in activation $V_{1/2}$ and depolarizing shift in inactivation $V_{1/2}$ at 35°C. These results are comparable to clinical observations while patient B (V1316A) presented with more severe symptoms as compared to the patients with the other two mutations. The depolarizing shift of voltage dependent activation observed in I848T mutant channel at 35°C is expected to counteract the depolarization in steady-state fast inactivation. However, the depolarization in activation does not result in further

depolarizing shift as compared with wild type channel at 35°C and it is possible that the shift in steady-state fast inactivation alone contributes to the disease phenotype. The results could also be explained by the contribution of sympathetic nervous system, where Na_v1.7 is also expressed abundantly (Toledo-Aral et al. 1997). Recent report has shown that neuropathic pain is resulted from the interaction between sympathetic and sensory neurons (Minett et al. 2012). The effects of indifference and depolarizing shift of activation observed in I136V and I848T may be implicated in sympathetic neurons. Further characterizations in whether these mutations produce hyper- or hypo-excitability in sympathetic neurons, and how they interact with the hyperexcitable sensory neurons will help elucidate the pathophysiology of PE.

4.4 Drug antagonism

The differential inhibitions of clinically available medications for PE were tested on wild type and mutant Na_v1.7 channels. We evaluated the concentration of 50% inhibition (IC₅₀) of sodium channel blockers lidocaine and mexiletine on wild type and mutant Na_v1.7 channels. The significant higher IC₅₀ values for lidocaine observed in I136V, I848T, and V1316A mutant Na_v1.7 channels suggest that lidocaine might not be a suitable treatment choice for patients with these mutations. In testing the mexiletine, only I848T mutant channel revealed a significant lower IC₅₀ as compared with wild type

channel. This result is compatible with the clinical observation that the visual analogue scale decreased in patient A (I848T) but not patient B (V1316A) after the mexiletine treatment (Fig. 12). Although similar improvement was also observed in the patient carrying I136V mutation, there was no significant difference in IC_{50} as compared with wild type channel (Fig. 12B). Previous study on another PE relating mutation, V872G showed similar IC_{50} for mexiletine but exhibited greater use-dependent current fall-off as compared with wild type channel (Choi et al. 2009)³. However, no difference was observed in our mutant channels compared with wild type channel in use-dependent assay (Fig. 13). Considering the disease phenotype might be resulted from interactions between sympathetic and sensory neurons (Minett et al. 2012), treatments that aim to attenuate the activity of $Na_v1.7$ in sensory neurons would be expected to be only partially effective. Although our results do not completely match the clinical observation, our method to some degree can still provide a quick screen for potential treatments for these patients.

4.5 Conclusion and future development

Results from our study showed that the I136V, I848T, and V1316A mutant $Na_v1.7$ channels exhibit altered electrophysiological properties that result in channel hyper-activity, which confers to the hyperexcitability in sensory neurons. Furthermore,

we demonstrated that at higher temperature (35°C), which would triggers PE symptoms, the hypersensitivity of mutant channels was enhanced and resulting in disease phenotype such as neuralgia and causalgia. Characterization of these mutant $\text{Na}_v1.7$ channels in sensory and sympathetic neurons and further investigation of the temperature effects on these neurons would be a direction for future studies.



References

- Ahn, H. et al., 2010. A new Nav1.7 sodium channel mutation I234T in a child with severe pain. *EUROPEAN JOURNAL OF PAIN*, p.1-7.
- Babb, R.R., Alarcon-Segovis, D. & Fairbairn, J.F., 1964. ERYTHERMALGIA. REVIEW OF 51 CASES. *Circulation*, 29, p.136-141.
- Burns, T.M. et al., 2005. Genetic heterogeneity and exclusion of a modifying locus at 2q in a family with autosomal dominant primary erythromelgia. *The British journal of dermatology*, 153(1), p.174-177.
- Catterall, W.A., 2000. From ionic currents to molecular mechanisms: the structure and function of voltage-gated sodium channels. *Neuron*, 26(1), p.13-25.
- Catterall, W.A. et al., 2005. International Union of Pharmacology. XLVII. Nomenclature and Structure-Function Relationships of Voltage-Gated Sodium Channels. *Pharmacological Reviews*, 57(4), p.397-409.
- Cheng, X et al., 2011. Deletion mutation of sodium channel NaV1.7 in inherited erythromelgia: enhanced slow inactivation modulates dorsal root ganglion neuron hyperexcitability. *Brain*, 134(7), p.1972-1986.
- Cheng, Xiaoyang et al., 2008. Mutation I136V alters electrophysiological properties of the NaV1.7 channel in a family with onset of erythromelgia in the second decade. *Molecular Pain*, 4(1), p.1.

- Cheng, Xiaoyang et al., 2010. Mutations at opposite ends of the DIII/S4-S5 linker of sodium channel Na V 1.7 produce distinct pain disorders. *Molecular Pain*, 6, p.24.
- Choi, J. et al., 2009. Mexiletine-responsive erythromelgia due to a new Nav1.7 mutation showing use-dependent current fall-off. *Experimental Neurology*, 216(2), p.383-389.
- Choi, J. et al., 2010a. Paroxysmal extreme pain disorder: a molecular lesion of peripheral neurons. *Nature Publishing Group*, 7(1), p.51-55.
- Choi, J.S. et al., 2010b. Alternative splicing may contribute to time-dependent manifestation of inherited erythromelgia. *Brain*, 133(6), p.1823-1835.
- Choi, J.S., Dib-Hajj, S.D. & Waxman, S.G., 2006. Inherited erythromelgia: Limb pain from an S4 charge-neutral Na channelopathy. *Neurology*, 67(9), p.1563-1567.
- Cox, J.J. et al., 2006. An SCN9A channelopathy causes congenital inability to experience pain. *Nature*, 444(7121), p.894-898.
- Cummins, T.R., Dib-Hajj, S.D. & Waxman, S.G., 2004. Electrophysiological Properties of Mutant Nav1.7 Sodium Channels in a Painful Inherited Neuropathy. *Journal of Neuroscience*, 24(38), p.8232-8236.
- Cummins, T.R., Howe, J.R. & Waxman, S.G., 1998. Slow closed-state inactivation: a novel mechanism underlying ramp currents in cells expressing the hNE/PN1

- sodium channel. *The Journal of neuroscience : the official journal of the Society for Neuroscience*, 18(23), p.9607-9619.
- Davis, M.D. et al., 2000. Natural history of erythromelalgia: presentation and outcome in 168 patients. *Archives of Dermatology*, 136(3), p.330-336.
- Dib-Hajj, S.D. et al., 2007. From genes to pain: Nav1.7 and human pain disorders. *Trends in Neurosciences*, 30(11), p.555-563.
- Dib-Hajj, S.D. et al., 2006. Mutations in the sodium channel Nav1.7 underlie inherited erythromelalgia. *Drug Discovery Today: Disease Mechanisms*, 3(3), p.343-350.
- Djoughri, L. et al., 2003. Sensory and electrophysiological properties of guinea-pig sensory neurones expressing Nav 1.7 (PN1) Na⁺ channel alpha subunit protein. *The Journal of Physiology*, 546(Pt 2), p.565-576.
- Drenth, J.P. et al., 2001. The primary erythromelalgia-susceptibility gene is located on chromosome 2q31-32. *American journal of human genetics*, 68(5), p.1277-1282.
- Drenth, J.P.H. & Waxman, S.G., 2007. Mutations in sodium-channel gene SCN9A cause a spectrum of human genetic pain disorders. *The Journal of clinical investigation*, 117(12), p.3603-3609.
- Drenth, J.P.H. et al., 2005. SCN9A mutations define primary erythromelalgia as a neuropathic disorder of voltage gated sodium channels. *The Journal of investigative dermatology*, 124(6), p.1333-1338.

- Drenth, J.P.H., van Genderen, P.J.J. & Michiels, J.J., 1994. Thrombocythemic Erythromelalgia, Primary Erythermalgia, and Secondary Erythermalgia: Three Distinct Clinicopathologic Entities. *Angiology*, 45(6), p.451-454.
- Estacion, M. et al., 2010. Can robots patch-clamp as well as humans? Characterization of a novel sodium channel mutation. *The Journal of Physiology*, 588(Pt 11), p.1915-1927.
- Faber, C.G. et al., 2011. Gain of function Nav1.7 mutations in idiopathic small fiber neuropathy. *Annals of Neurology*, p.26-39.
- Fertleman, C R & Ferrie, C.D., 2006. What's in a name--familial rectal pain syndrome becomes paroxysmal extreme pain disorder. *Journal of Neurology, Neurosurgery & Psychiatry*, 77(11), p.1294-1295.
- Fertleman, C R et al., 2007. Paroxysmal extreme pain disorder (previously familial rectal pain syndrome). *Neurology*, 69(6), p.586-595.
- Fertleman, Caroline R et al., 2006. SCN9A mutations in paroxysmal extreme pain disorder: allelic variants underlie distinct channel defects and phenotypes. *Neuron*, 52(5), p.767-774.
- Fischer, T.Z. et al., 2009. A novel Nav1.7 mutation producing carbamazepine-responsive erythromelalgia. *Annals of Neurology*, 65(6), p.733-741.

- Han, C et al., 2009. Early- and late-onset inherited erythromelalgia: genotype-phenotype correlation. *Brain*, 132(7), p.1711-1722.
- Han, Chongyang et al., 2006. Sporadic onset of erythromelalgia: a gain-of-function mutation in Nav1.7. *Annals of Neurology*, 59(3), p.553-558.
- Han, Chongyang et al., 2007. Temperature dependence of erythromelalgia mutation L858F in sodium channel Nav1.7. *Molecular Pain*, 3(1), p.3.
- Harty, T.P. et al., 2006. Nav1.7 Mutant A863P in Erythromelalgia: Effects of Altered Activation and Steady-State Inactivation on Excitability of Nociceptive Dorsal Root Ganglion Neurons. *Journal of Neuroscience*, 26(48), p.12566-12575.
- Hisama FM, Dib-Hajj SD, Waxman SG. SCN9A-Related Inherited Erythromelalgia. 2006 May 6 [Updated 2008 Sep 25]. In: Pagon RA, Bird TD, Dolan CR, et al., editors. GeneReviews™ [Internet]. Seattle (WA): University of Washington, Seattle; 1993-.
- Lampert, A. et al., 2009. Erythromelalgia mutation L823R shifts activation and inactivation of threshold sodium channel Nav1.7 to hyperpolarized potentials. *Biochemical and Biophysical Research Communications*, 390(2), p.319-324.
- Lampert, A. et al., 2006. Size matters: Erythromelalgia mutation S241T in Nav1.7 alters channel gating. *Journal of Biological Chemistry*, 281(47), p.36029-36035.

- Lee, M. et al., 2007. Characterization of a familial case with primary erythromelalgia from Taiwan. *Journal of Neurology*, 254(2), p.210-214.
- Minett, M.S. et al., 2012. Distinct Nav1.7-dependent pain sensations require different sets of sensory and sympathetic neurons. *Nature Communications*, 3, p.791-9.
- Mitchell, W.S., 1878. Article I. On a Rare Vaso-motor Neurosis of the Extremities,1 and on the Maladies with which it may be confounded. *The American Journal of the Medical Sciences*, 151, p.17‐36.
- Natkunarahaj, J., et al., 2009. Treatment with carbamazepine and gabapentin of a patient with primary erythromelalgia (erythromelalgia) identified to have a mutation in the SCN9A gene, encoding a voltage-gated sodium channel. *Clinical and experimental dermatology*, 34(8), p. e640-e642.
- Rogers, M. et al., 2006. The role of sodium channels in neuropathic pain. *Seminars in Cell & Developmental Biology*, 17(5), p.571-581.
- Rush, A.M. et al., 2006. A single sodium channel mutation produces hyper- or hypoexcitability in different types of neurons. *Proceedings of the National Academy of Sciences of the United States of America*, 103(21), p.8245-8250.
- Seneschal, J. et al., 2009. A case of primary erythromelalgia with encephalopathy. *Journal of Neurology*, 256(10), p.1767-1768.

Thompson, G.H., Hahn, G. & Rang, M., 1979. Erythromelalgia. *Clinical orthopaedics and related research*, (144), p.249-254.

Toledo-Aral, J.J. et al., 1997. Identification of PN1, a predominant voltage-dependent sodium channel expressed principally in peripheral neurons. *Proceedings of the National Academy of Sciences of the United States of America*, 94(4), p.1527-1532.

Wang, W. et al., 2011. Are voltage-gated sodium channels on the dorsal root ganglion involved in the development of neuropathic pain? *Molecular Pain*, 7(1), p.16.

Waxman, S.G. & Dib-Hajj, S., 2005. Erythermalgia: molecular basis for an inherited pain syndrome. *Trends in Molecular Medicine*, 11(12), p.555-562.

Weiss, J. et al., 2011. Loss-of-function mutations in sodium channel Nav1.7 cause anosmia. *Nature*, 472(7342), p.186-190.

West, J.W. et al., 1992. A cluster of hydrophobic amino acid residues required for fast Na(+)-channel inactivation. *Proceedings of the National Academy of Sciences of the United States of America*, 89(22), p.10910-10914.

Wood, J.N. et al., 2004. Voltage-gated sodium channels and pain pathways. *Journal of Neurobiology*, 61(1), p.55-71.

Yang, Y. et al., 2004. Mutations in SCN9A, encoding a sodium channel alpha subunit, in patients with primary erythermalgia. *Journal of Medical Genetics*, 41(3), p.171-174.

Yarov-Yarovoy, V. et al., 2012. Structural basis for gating charge movement in the voltage sensor of a sodium channel. *Proceedings of the National Academy of Sciences*, 109(2), p.E93-102.

Zhang, L. et al., 2007. Mutation hotspots of SCN9A in primary erythralgia. *The British journal of dermatology*, 156(4), p.767-769.



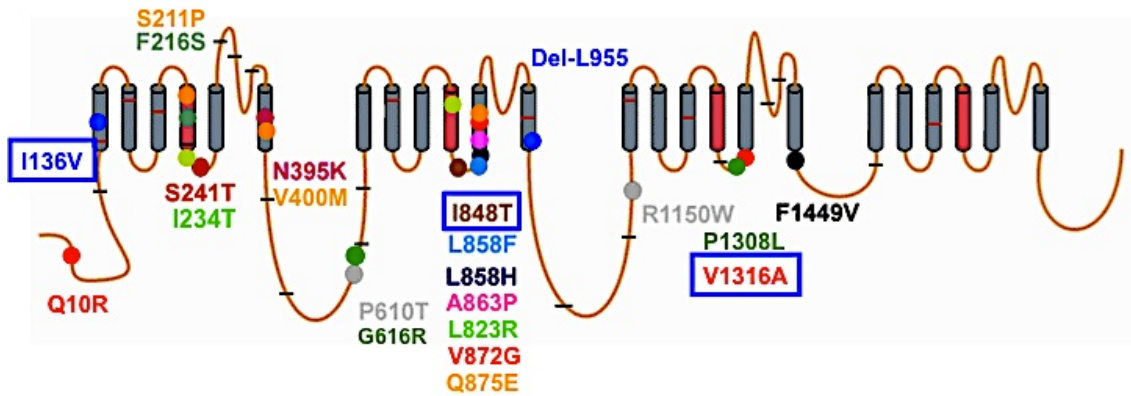


Figure 1. Schematic drawing of human Na_v1.7 showing all the mutations related to primary erythromelalgia, which include 19 missense mutations and one in-frame deletion mutation. The gray annotations are polymorphisms that are not directly linked with PE. Mutations analyzed in this study are denoted with blue boxes. (This figure is modified from a figure previously published by Waxman and Dig-Hajj (2005) in “Erythromelalgia: molecular basis for an inherited pain syndrome”, Trends in Molecular Medicine, 11(12), 555-562.)

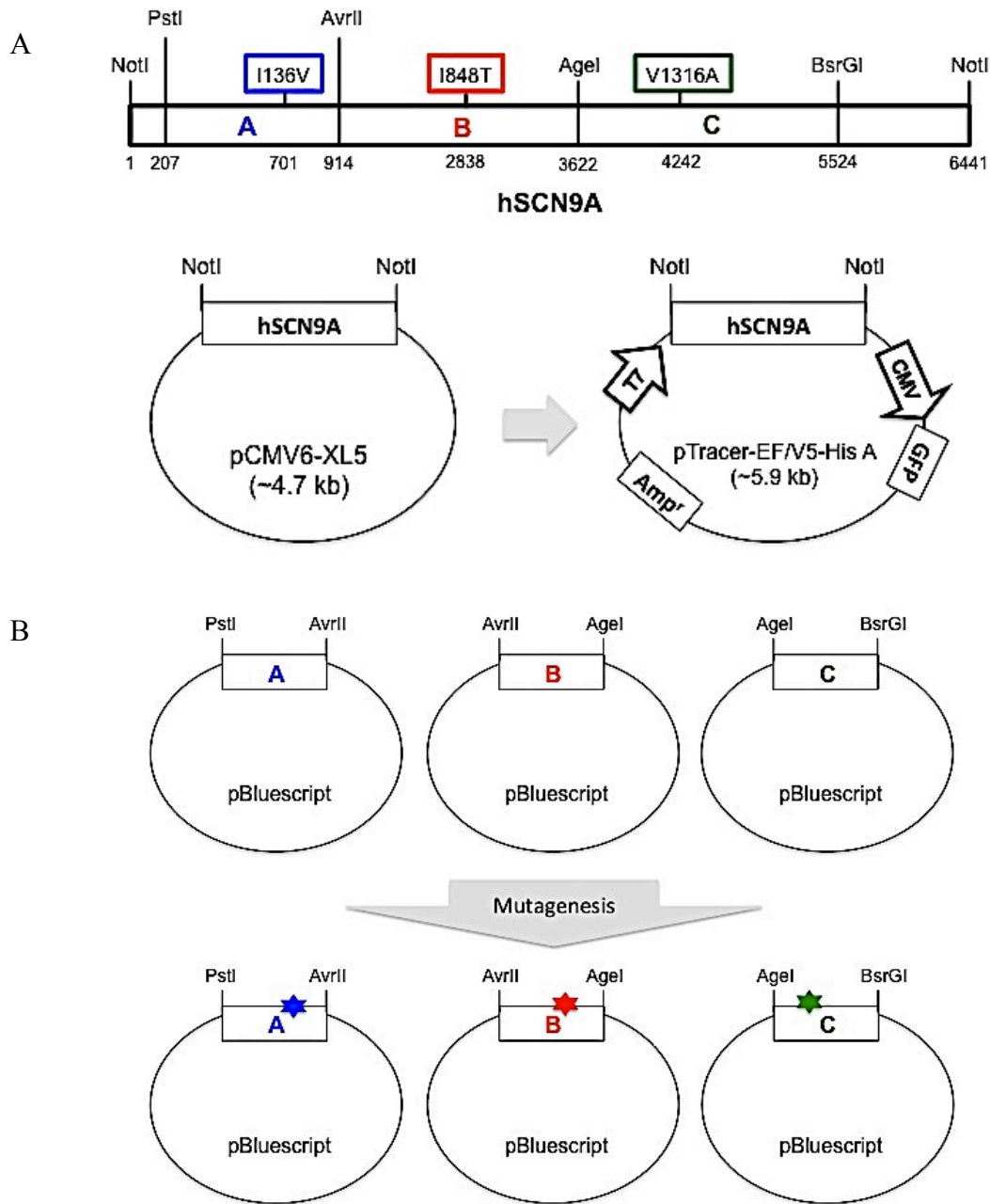
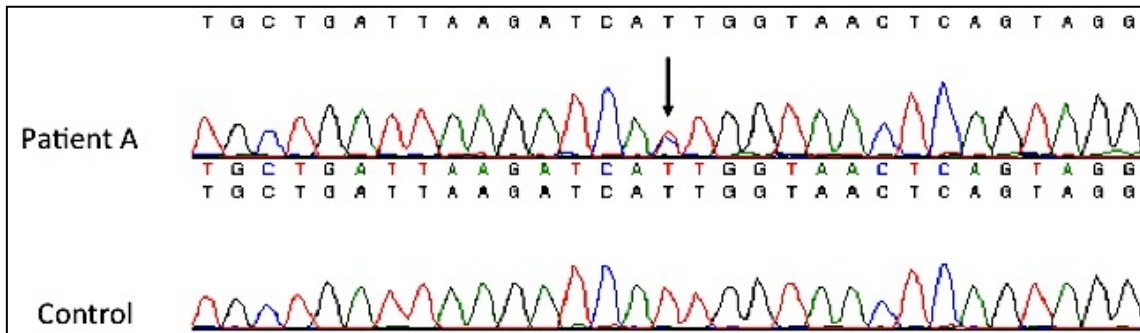


Figure 2. Cloning strategies of hSCN9A full-length cDNA. (A) The positions of mutations are labeled in blue (I1376V), red (I848T), and green (V1316A) boxes along with the selected restriction enzyme sites. Full-length hSCN9A was cloned into pTracer-EF/V5-His A vector using NotI cutting sites. (B) Fragments A/B/C containing mutation points were subcloned into pBluescript using indicated restriction enzymes

(PstI/AvrII for fragment A; AvrII/AgeI for fragment B; AgeI/BsrGI for fragment C) for mutagenesis. Following successful mutagenesis, each mutation-containing fragment was cloned back to pTracer-hSCN9A.



A



B

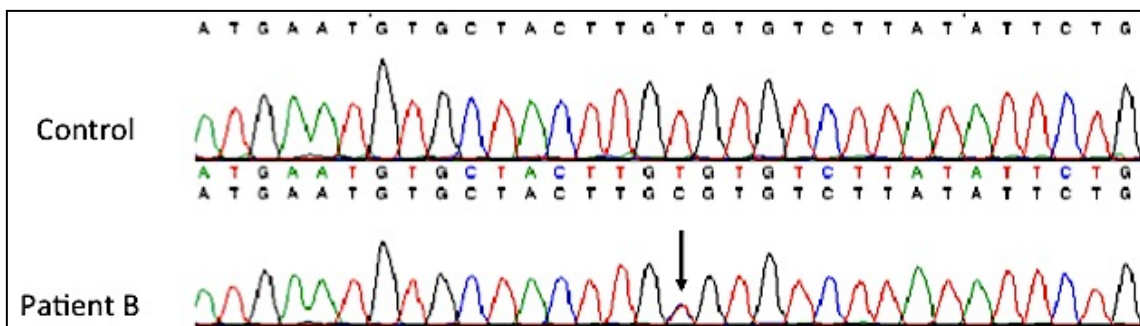


Figure 3. Sequence chromatography of patients carrying (A) I848T and (B) V1316A mutations in *SCN9A* gene. (A) A point mutation c.2543T>C in exon 15 results in a missense mutation of isoleucine 848 changed to threonine was found in patient A. (B) In patient B, a point missense mutation of c.3947T>C in exon 22 results in valine 1316 changed to alanine.

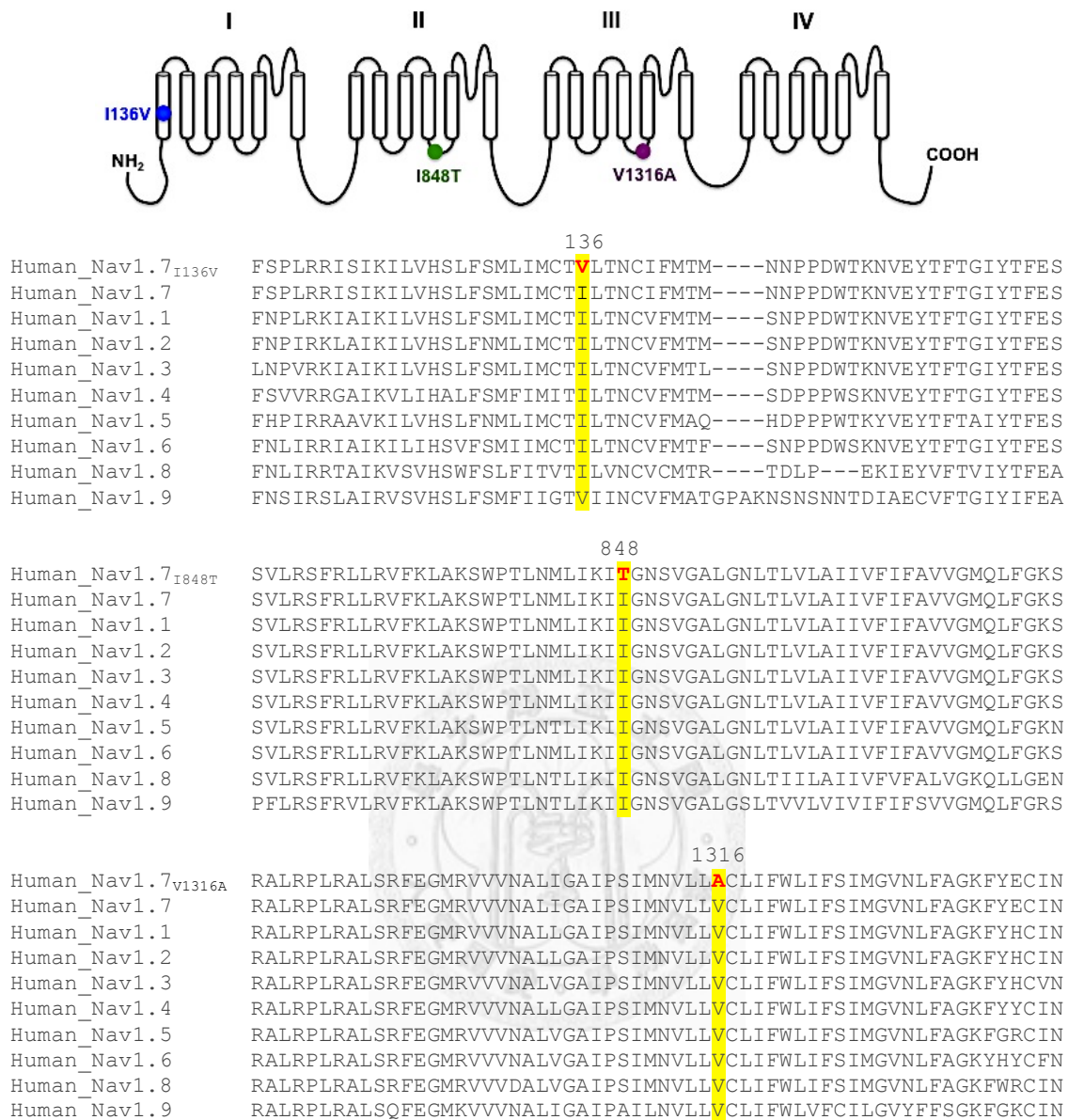


Figure 4. Topological drawing of Nav1.7 protein showing the positions of I136V, I848T, and V1316A mutations (top panel) and protein sequence alignments with other human sodium channel subtypes at the positions (text in red and highlighted in yellow).

	136
Human_Nav1.7 _{I136V}	FSPLRRISIKILVHS--LFSMLIMCTVLTNCIFMTMNNPPDWTKNVEYFTFTGIYTFESL
Human_Nav1.7	FSPLRRISIKILVHS--LFSMLIMCTILTNCIFMTMNNPPDWTKNVEYFTFTGIYTFESL
Mouse_Nav1.7	FSPLRRISIKILVHS--LFSMLIMCTILTNCIFMTMSNPPDWTKNVEYFTFTGIYTFESL
Rat_Nav1.7	FSPLRRISIKILVHS--LFSMLIMCTILTNCIFMTLSNPPPEWTKNVEYFTFTGIYTFESL
Chimpanzee_Nav1.7	FSPLRRISIKILVHS--TLFSMLIMCTILTNCIFMTMNNPPDWTKNVEYFTFTGIYTFESL
Dog_Nav1.7	FSPLRRISIKILVHSSTLFSMLIMCTILTNCIFMTMSNPPDWTKNVEYFTFTGIYTFESL
Naked Mole Rat_Nav1.7	FSPLRRISIKILVHS--LFSMLIMCTILTNCIFMTMSSPPEWTKNVEYFTFTGIYTFESL
	848
Human_Nav1.7 _{I848T}	SVLRSFRLLRVFKLAKSWPTLNMLIKITGNSVGALGNLTLVLAIIVFIFAVVGMQLFGK
Human_Nav1.7	SVLRSFRLLRVFKLAKSWPTLNMLIKITGNSVGALGNLTLVLAIIVFIFAVVGMQLFGK
Mouse_Nav1.7	SVLRSFRLLRVFKLAKSWPTLNMLIKITGNSVGALGNLTLVLAIIVFIFAVVGMQLFGK
Rat_Nav1.7	SVLRSFRLLRVFKLAKSWPTLNMLIKITGNSVGALGNLTLVLAIIVFIFAVVGMQLFGK
Chimpanzee_Nav1.7	SVLRSFRLLRVFKLAKSWPTLNMLIKITGNSVGALGNLTLVLAIIVFIFAVVGMQLFGK
Dog_Nav1.7	SVLRSFRLLRVFKLAKSWPTLNMLIKITGNSVGALGNLTLVLAIIVFIFAVVGMQLFGK
Naked Mole Rat_Nav1.7	SVLRSFRLLRVFKLAKSWPTLNMLIKITGNSMGALGNLTLVLAIIVFIFAVVGMQLFGK
	1316
Human_Nav1.7 _{V1316A}	RALRPLRALSREFEGMRVVVNALIGAIPSIMNVLLVCLIFWLIFSIMGVNLFAGKFYECI
Human_Nav1.7	RALRPLRALSREFEGMRVVVNALIGAIPSIMNVLLVCLIFWLIFSIMGVNLFAGKFYECI
Mouse_Nav1.7	RALRPLRALSREFEGMRVVVNALIGAIPSIMNVLLVCLIFWLIFSIMGVNLFAGKFYECV
Rat_Nav1.7	RALRPLRALSREFEGMRVVVNALIGAIPSIMNVLLVCLIFWLIFSIMGVNLFAGKFYECV
Chimpanzee_Nav1.7	RALRPLRALSREFEGMRVVVNALIGAIPSIMNVLLVCLIFWLIFSIMGVNLFAGKFYECI
Dog_Nav1.7	RALRPLRALSREFEGMRVVVNALIGAIPSIMNVLLVCLIFWLIFSIMGVNLFAGKFYECV
Naked Mole Rat_Nav1.7	RALRPLRALSREFEGMRVVVNALIGAIPSIMNVLLVCLIFWLIFSIMGVNLFAGKFYECV

Figure 5. Na_v1.7 protein sequence alignments of mutation positions (text in red and highlighted in yellow) with Na_v1.7 homologs of various species.

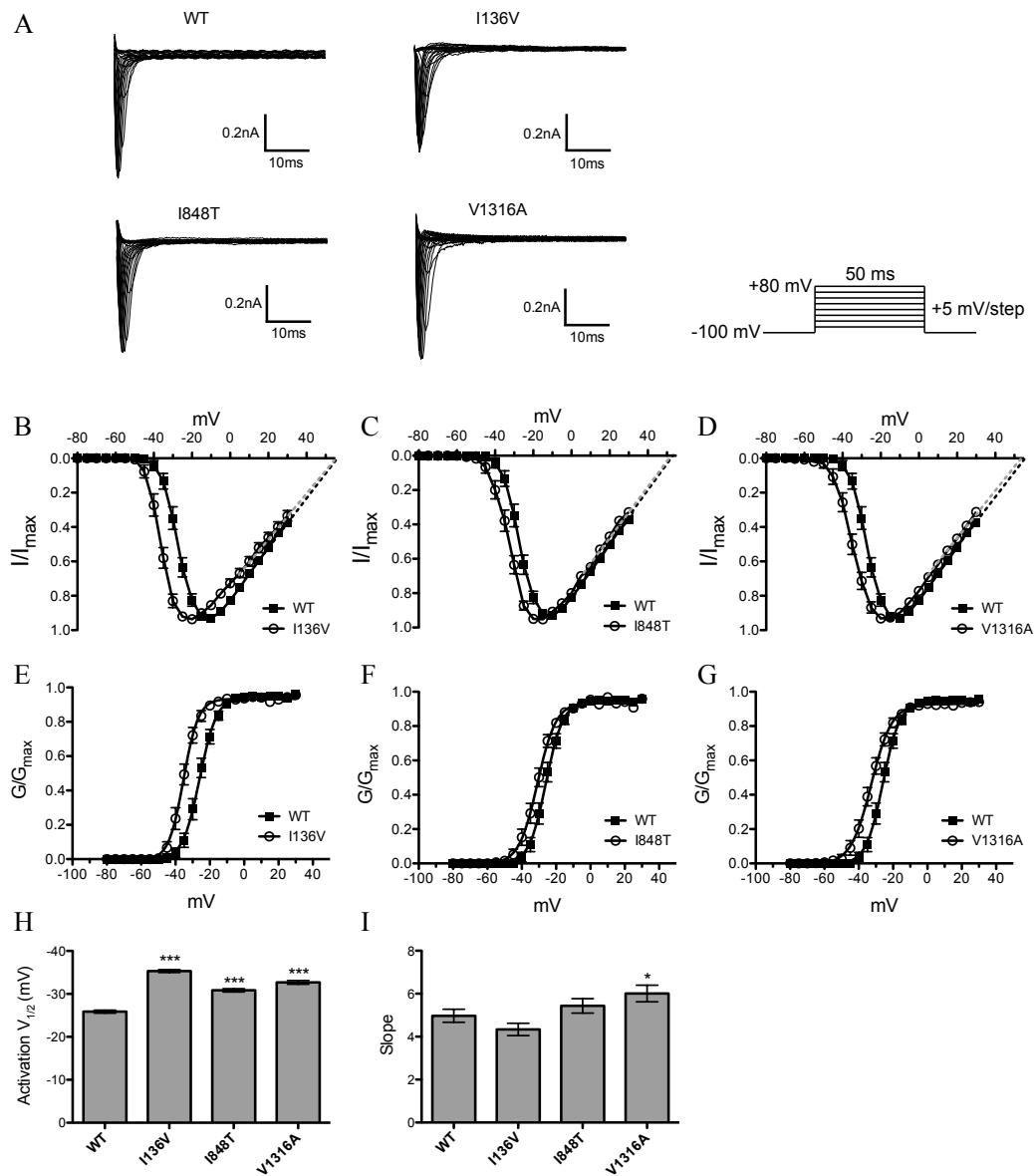


Figure 6. Current-voltage relationships of wild type and mutant $\text{Na}_v1.7$ channels. (A) Representative current traces showed no apparent differences between wild type and mutant channels. The current-voltage curves (B-D) showed a hyperpolarizing shift in activation in all mutant (empty circles) channels without shifting in reversal potential as compared with wild type (solid squares). (H) The activation $V_{1/2}$ of wild type channel is

about -25.88 mV, -35.32 mV for I136V, -30.84 mV for I848T, and -32.68 mV for V1316A mutant channel. (I) V1316A mutant channel show an increase in slope factor and no difference in I136V and I848T mutant channels as compared with wild type. (*P < 0.05, ***P < 0.001 vs. wild type; t-test; data shown as means \pm SEM)



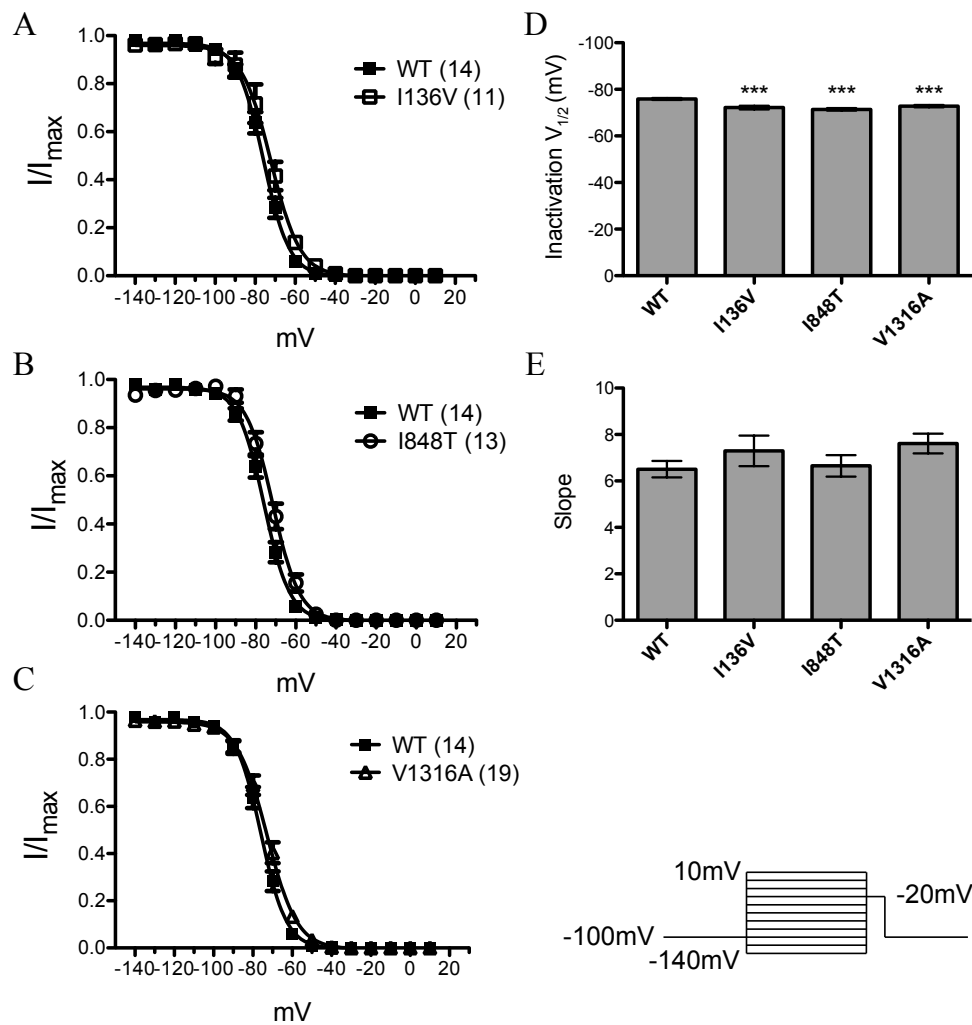


Figure 7. Steady-state fast inactivation curves of wild type and mutant $Na_v1.7$ channels.

(A) I136V, (B) I848T, and (C) V1316A mutant channels produce a significant depolarizing shift in inactivation $V_{1/2}$ as compared with wild type channel. (D) Inactivation $V_{1/2}$ of wild type channel is about -75.9 mV and mutant channels produce ~3.7 mV depolarizing shift for I136V, ~4.5 mV for I848T, and ~3.1mV for V1316A. (E) There is no significant difference in slopes. (***) $P < 0.001$ vs. wild type; t-test; means \pm SEM)

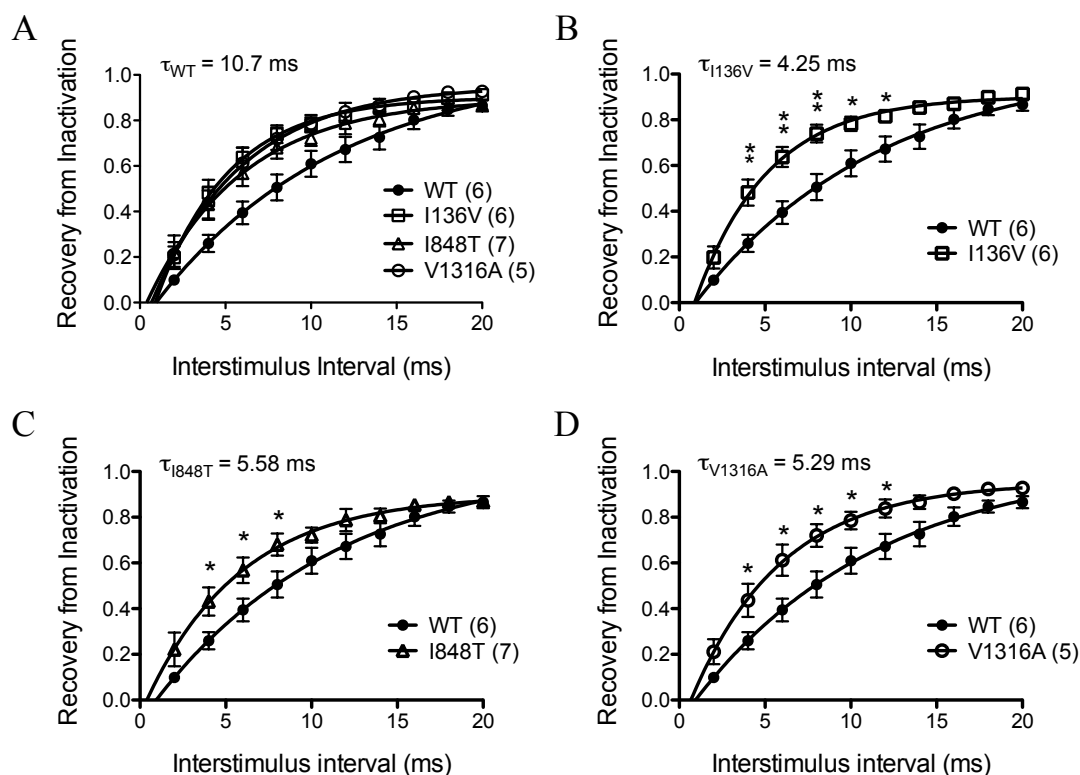


Figure 8. (A) Inactivation recovery rate of wild type (solid circles) and mutant (empty symbols) $\text{Na}_v1.7$ channels. Recovery time constant, $\tau = 10.7$ ms for wild type channel. (B)(D) I136V and V1316A mutant channels have significant faster recovery from inactivation between interstimulus interval of 4-10 ms and have a recovery τ of 4.25 ms and 5.29 ms, respectively. (C) I848T mutant channel recovers from inactivation significantly faster than wild type between 4-6 ms of interstimulus interval with a recovery τ , 5.58 ms. (N numbers are annotated in parentheses; * $P < 0.05$, ** $P < 0.01$ vs. wild type; t-test; data shown as means \pm SEM)

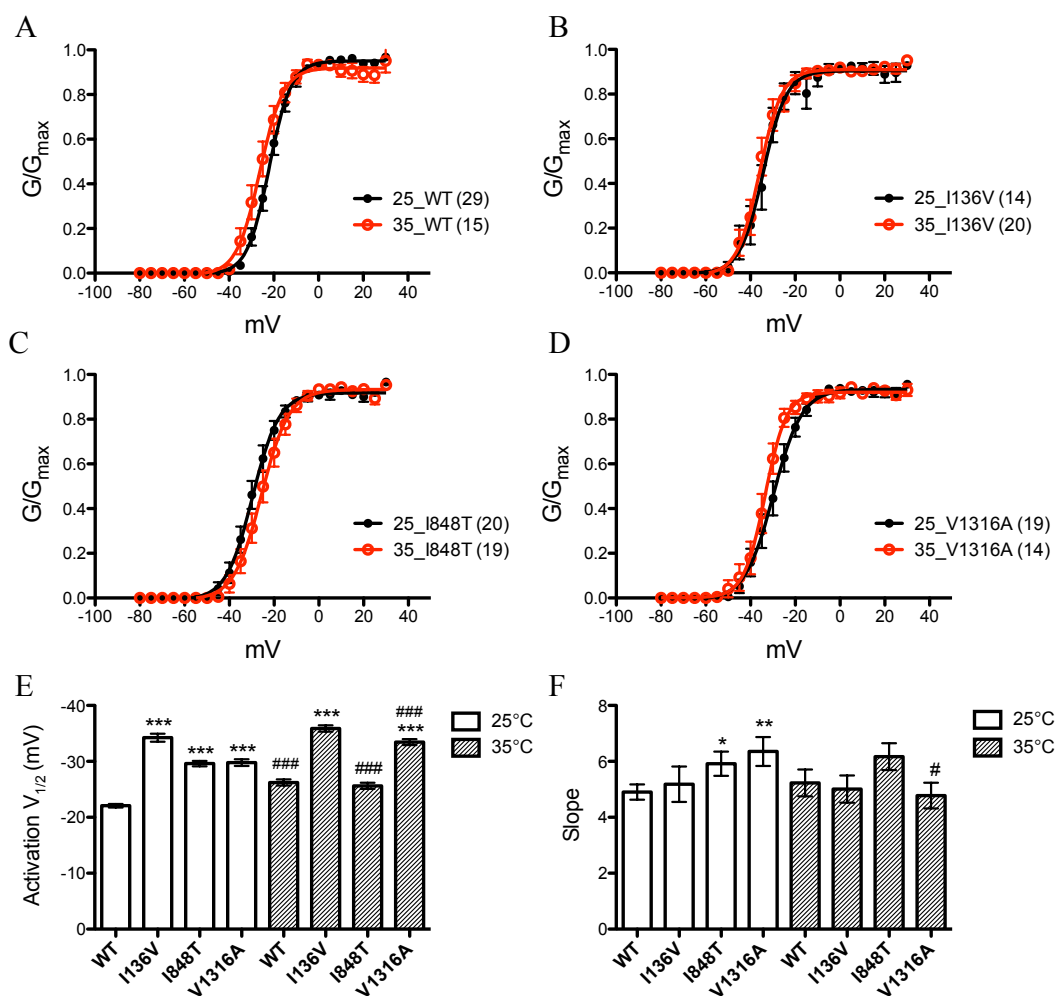


Figure 9. Activation curves of (A) wild type and (B) I136V, (C) I848T, (D) V1316A mutant channels at 25°C (black curves) and 35°C (red curves). (E) Wild type and V1316A mutant channels show a hyperpolarizing shift (WT: \sim 4.2 mV; V1316A: \sim 3.7 mV) in activation $V_{1/2}$ at 35°C compared with 25°C, while I136V is unchanged. I848T mutant channel shows a depolarizing shift (\sim 4 mV) at 35°C. All activation $V_{1/2}$ of mutant channels are more hyperpolarized than wild type at 25°C. (F) The slope of V1316A significantly reduces at 35°C as compared with 25°C. (* $P < 0.05$, ** $P < 0.01$,

***P < 0.001 vs. wild type; #P < 0.05, ###P < 0.001 vs. 35°C; t-test; data shown as means \pm SEM)



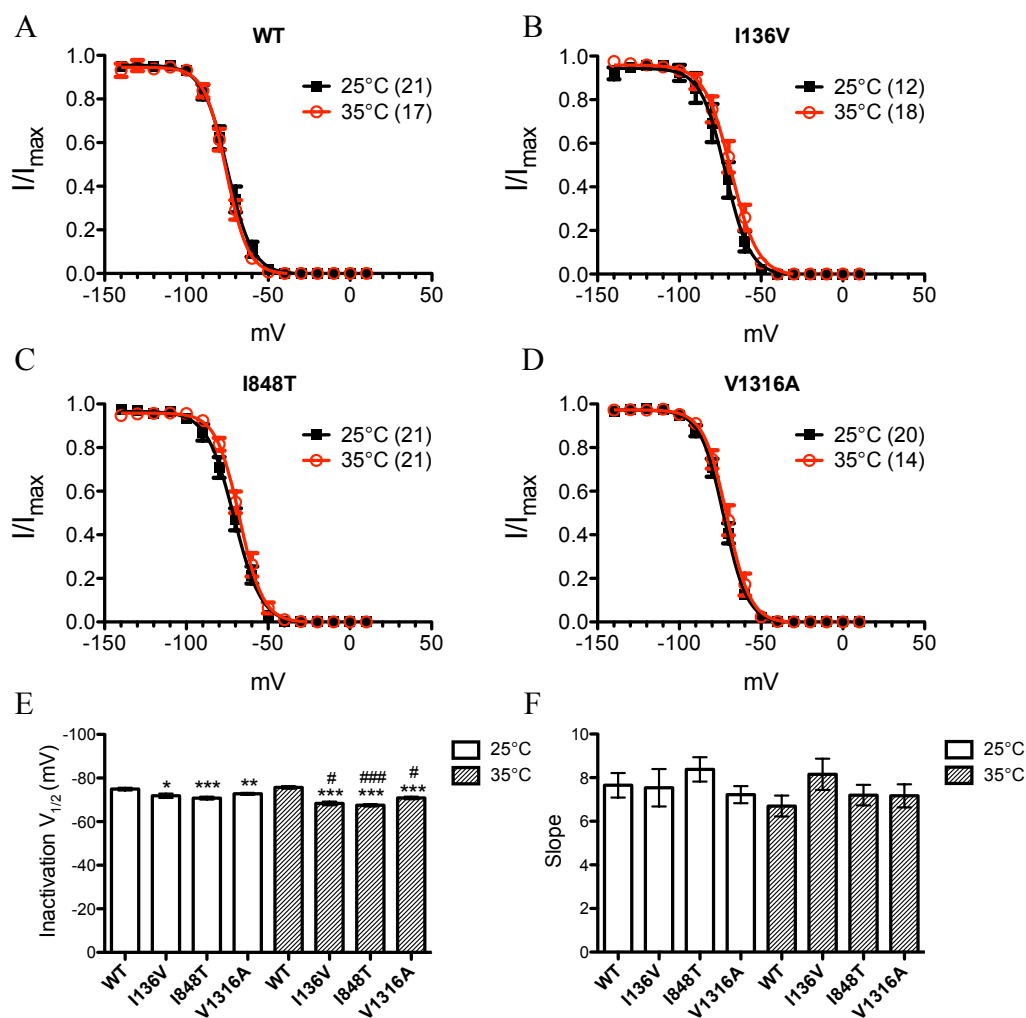


Figure 10. Steady-state fast inactivation curves of (A) wild type and (B) I136V, (C) I848T, (D) V1316A mutant channels at 25°C (black curves) and 35°C (red curves). (E) No significant difference in inactivation $V_{1/2}$ of wild type channel between 25°C and 35°C. At 35°C all mutant channels produce a significantly more depolarized inactivation $V_{1/2}$ compared with 25°C. (F) There is no significant difference in slopes. (* $P < 0.05$, ** $P < 0.01$, *** $P < 0.001$ vs. wild type; # $P < 0.05$, ### $P < 0.001$ vs. 35°C; t-test; data shown as means \pm SEM)

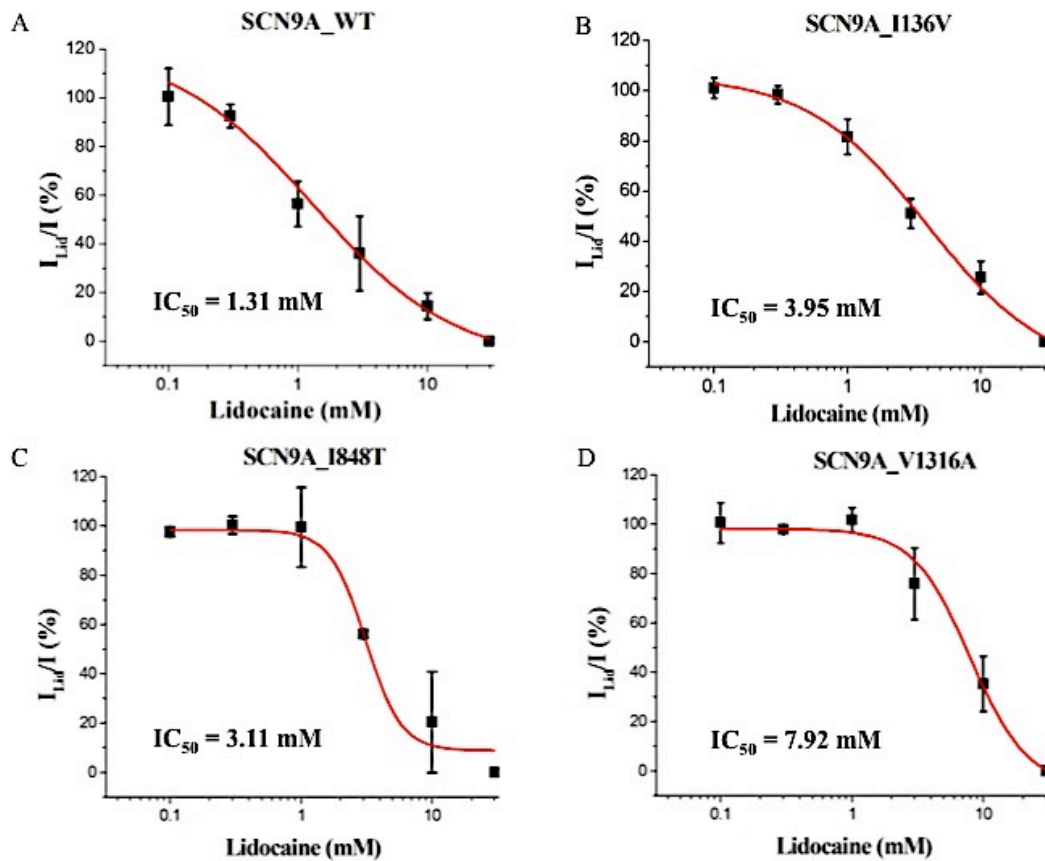


Figure 11. Lidocaine IC_{50} curves of (A) wild type, (B) I136V, (C) I848T, and (D) V1316A mutant $Na_v1.7$ channels. The IC_{50} value of wild type channel for lidocaine is 1.31 ± 0.87 mM. All the mutant channels reveal significant higher IC_{50} values (I136V: 3.95 ± 1.58 mM^{**}; I848T: 3.11 ± 0.48 mM^{*}; V1316A: 7.92 ± 2.50 mM^{***}) compared with wild type. (N = wild type: 5, I136V: 7, I848T: 3, V1316A: 4; ^{*}P < 0.05, ^{**}P < 0.01, ^{***}P < 0.001 vs. wild type; t-test; data shown as means \pm SEM)

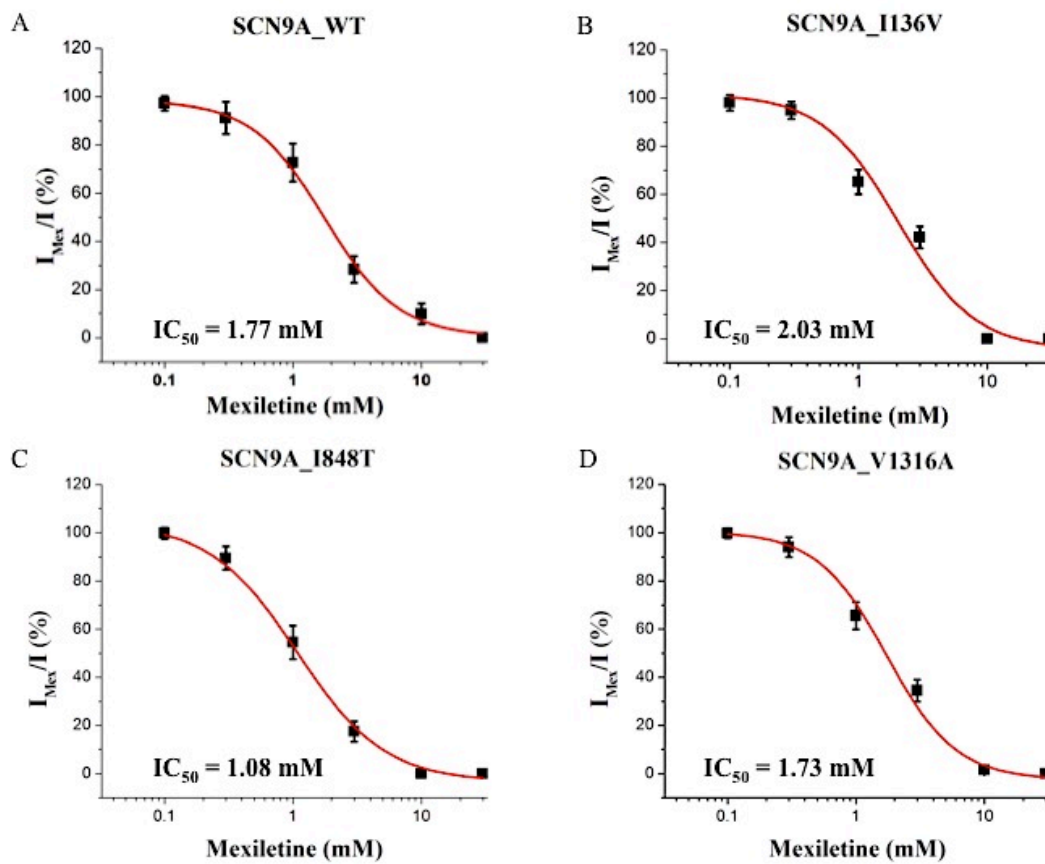
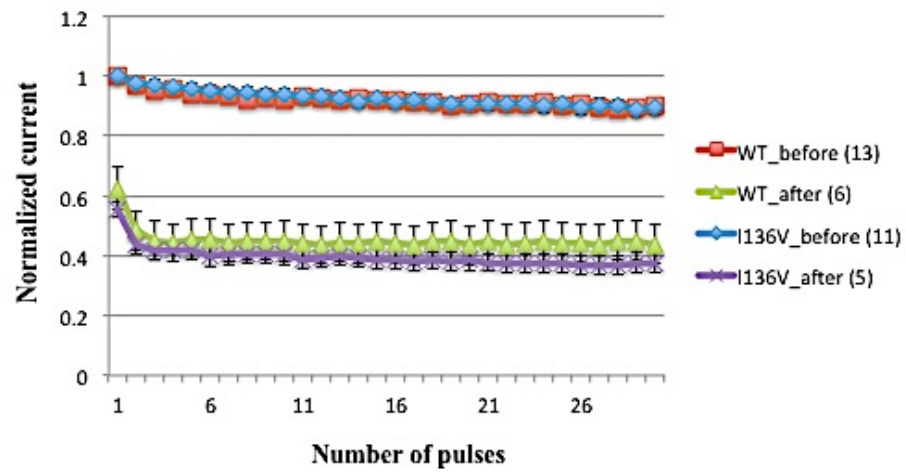
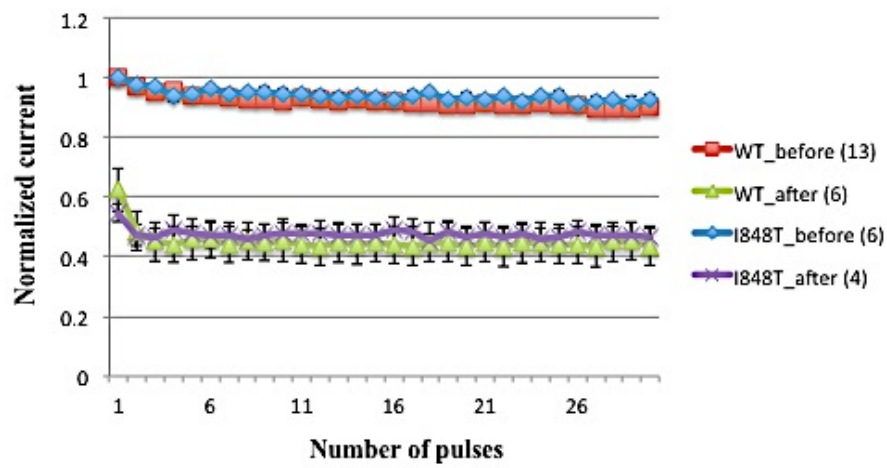


Figure 12. Mexiletine IC_{50} curves of (A) wild type, (B) I136V, (C) I848T, and (D) V1316A mutant Na_v1.7 channels. The IC_{50} value of wild type channel for mexiletine is 1.77 ± 0.78 mM. No significant difference in IC_{50} values of I136V (2.03 ± 0.38 mM) and V1316A (1.73 ± 0.20 mM) mutant channels compared with wild type channel. I848T mutant has a significant ($P < 0.05$) lower IC_{50} value (1.08 ± 0.11 mM) compared with wild type channel. (N = wild type: 6, I136V: 7, I848T: 7, V1316A: 8; t-test; data shown as means \pm SEM)

A



B



C

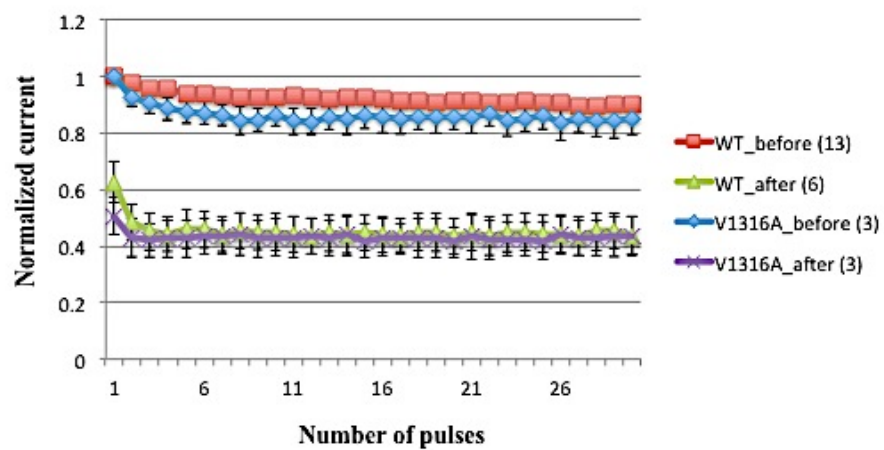


Figure 13. Use-dependent effect of mexiletine on wild type and (A) I136V, (B) I848T, (C) V1316A mutant $\text{Na}_v1.7$ channels before and after treatment of 1 mM of mexiletine.

N numbers are annotated in parentheses.

25°C						
Na _v 1.7	V _{1/2, act}	Slope	n	V _{1/2, inact}	Slope	n
WT	-22.07 ± 0.31	4.90 ± 0.27	29	-74.92 ± 0.65	7.65 ± 0.56	21
I136V	-34.24 ± 0.72 ^{***}	5.18 ± 0.63	13	-71.84 ± 0.99 [*]	7.54 ± 0.87	12
I848T	-29.6 ± 0.50 ^{***}	5.92 ± 0.43 [*]	20	-70.78 ± 0.64 ^{***}	8.38 ± 0.56	21
V1316A	-29.78 ± 0.59 ^{***}	6.36 ± 0.52 ^{**}	19	-72.76 ± 0.45 ^{**}	7.22 ± 0.39	20

35°C						
Na _v 1.7	V _{1/2, act}	Slope	n	V _{1/2, inact}	Slope	n
WT	-26.22 ± 0.55 ^{###}	5.23 ± 0.48	15	-75.71 ± 0.55	6.70 ± 0.48	17
I136V	-35.89 ± 0.56 ^{***}	5.01 ± 0.49	20	-68.4 ± 0.82 ^{***, #}	8.16 ± 0.72	18
I848T	-25.62 ± 0.55 ^{###}	6.17 ± 0.48	19	-67.52 ± 0.54 ^{***, ###}	7.20 ± 0.47	21
V1316A	-33.45 ± 0.53 ^{***, ###}	4.78 ± 0.46 [#]	14	-70.88 ± 0.61 ^{***, #}	7.17 ± 0.53	14

Table 1. Summary of electrophysiological properties of wild type and mutant Na_v1.7 channels at 25°C and 35°C. (*P < 0.05, **P < 0.01, ***P < 0.001 vs. WT; #P < 0.05, ###P < 0.01, ####P < 0.001 vs. 35°C; t-test; data shown as means ± SEM)

Domain	Mutations	HEK293 Cell					DRG neuron	
		Activation $V_{1/2}$	Inactivation $V_{1/2, \text{fast}}$	Inactivation $V_{1/2, \text{slow}}$	Deactivation	Ramp Current	AP threshold	Repetitive firing
I	I234T	Hyperpolarized	-	Hyperpolarized	Slowed	Increased	ND	ND
	S241T	Hyperpolarized	ND	Hyperpolarized	Slowed	Increased	ND	ND
II	I848T	Hyperpolarized	-	-	Slowed	Increased	Reduced	Enhanced
	L858H	Hyperpolarized	-	Hyperpolarized	Slowed	Increased	ND	ND
	L858F	Hyperpolarized	Depolarized	-	Slowed	Increased	Reduced	Enhanced
III	P1308L	Hyperpolarized	-	-	-	Increased	Reduced	Enhanced
	V1316A*	Hyperpolarized	Depolarized	ND	ND	ND	ND	ND

ND: Not determined

“-”: No difference compared with wild type.

* Novel mutation characterized in this study using CHO-K1 cells.

Table 2. Summary of $\text{Na}_v1.7$ mutations located at S4/S5 linker regions.



	Lidocaine (mM)	n	Mexiletine (mM)	n
WT	1.31 ± 0.87	5	1.77 ± 0.78	6
I136V	3.95 ± 1.58**	7	2.03 ± 0.38	7
I848T	3.11 ± 0.48*	3	1.08 ± 0.11*	7
V1316A	7.92 ± 2.50***	4	1.73 ± 0.20	8

Table 3. IC₅₀ values of lidocaine and mexiletine. (*P < 0.05, **P < 0.01, ***P < 0.001

vs. wild type; t-test; data shown as means ± SEM)



Appendix I

